Biology Direct

RESEARCH Open Access

FXR1 associates with and degrades PDZK1IP1 and ATOH8 mRNAs and promotes esophageal cancer progression

Faiz Ali Khan[1,2,3,4], Dalia Fouad[5], Farid S. Ataya[6], Na Fang[3*], Jingcheng Dong[1,2*] and Shaoping Ji[3,7*]

Abstract

Background The growing body of evidence suggests that RNA-binding proteins (RBPs) have an important function in cancer biology. This research characterizes the expression status of fragile X-related protein 1 (FXR1) in esophageal cancer (ESCA) cell lines and understands its mechanistic importance in ESCA tumor biology.

Methods The role of FXR1, PDZK1IP1, and ATOH8 in the malignant biological behaviors of ESCA cells was investigated using in-vitro and in-vivo experiments.

Results FXR1 was aberrantly overexpressed at both the transcript and protein levels in ESCA cells. Deficiency of FXR1 in ESCA cells was associated with decreased cell proliferation, viability and compromised cell migration compared to the control group. In addition, the inhibition of FXR1 leads to the promotion of apoptosis and cell cycle arrest in ESCA cells. Furthermore, FXR1 knockdown stabilizes senescence markers, promoting cellular senescence and decreasing cancer growth. Mechanistically, FXR1 negatively regulated *PDZK1IP1* or *ATOH8* transcripts by promoting mRNA degradation via direct interaction with its 3'UTR. PDZK1IP1 or ATOH8 overexpression predominantly inhibited the tumor-promotive phenotype in FXR1-overexpressed cells. Furthermore, FXR1 inhibition and PDZK1IP1 or ATOH8 overexpression in combination with FXR1-overexpressed cells significantly decreased xenograft tumor formation and enhanced nude mouse survival without causing apparent toxicity ($P < 0.01$). In the FXR1 knockdown group, the tumor weight of mice decreased by 80% compared to the control group ($p < 0.01$).

Conclusions Our results demonstrate FXR1's oncogenic involvement in ESCA cell lines, suggesting that FXR1 may be implicated in ESCA development by regulating the stability of *PDZK1IP1* and *ATOH8* mRNAs. For the first time, our findings emphasize the importance of FXR1-*PDZK1IP1* and -*ATOH8* functional modules in the development of ESCA, which might have potential diagnostic or therapeutic implications.

Keywords RNA binding proteins, FXR1, *PDZK1IP1*, *ATOH8*, Malignancy

*Correspondence:
Na Fang
fangna@henu.edu.cn
Jingcheng Dong
jcdong2004@126.com
Shaoping Ji
shaopingji@henu.edu.cn
[1]Department of Integrative Medicine, Huashan Hospital, Fudan University, Middle Urumqi Road, Shanghai, China
[2]Institutes of Integrative Medicine, Fudan University, Shanghai, China
[3]Laboratory of Cell Signal Transduction, Department of Biochemistry and Molecular Biology, School of Basic Medical Sciences, Henan University, Kaifeng, Henan 475004, China
[4]Department of Basic Sciences Research, Shaukat Khanum Memorial Cancer Hospital and Research Centre (SKMCH&RC), Lahore, Pakistan
[5]Department of Zoology, College of Science, King Saud University, Riyadh, Saudi Arabia
[6]Department of Biochemistry, College of Science, King Saud University, Riyadh, Saudi Arabia
[7]Center for Molecular Medicine, Faculty of Basic Medical Subjects, Shu-Qing Medical College of Zhengzhou, Zhengzhou, Henan, China

Background

Post-transcriptionally, RNA-binding proteins (RBPs) regulate the expression level of multiple target RNAs interacting with particular binding sites within the coding region (36%) or 3′-untranslated region (64%). The accumulating evidence suggests that RBP dysregulation plays a significant role in carcinogenesis. However, the role of fragile X-related protein 1 (FXR1) in cancers is just beginning to be revealed [1–4]. FXR1, located on chromosome 3q26–27, is a member of the Fragile X-Related (FXR) family of RBPs [5]. Several cancer-related genes are up/downregulated by FXR1 by modulating post-transcriptional and translational gene expression levels. FXR1 may control various transcripts processing due to the diversity of their RNA-binding domains and functional flexibility. FXR1 plays a role in mRNA transport, translation, and degradation by binding AU-rich elements (AREs) on RNA and G-quartet (Gq) regions [6–8]. In addition to being able to bind to RNA, FXR1 can also bind to free ribosomes and polyribosomes [9]. FXR1 is primarily found in the cytoplasm [10], but similar to several other RBPs, it can shuttle between the cytoplasm and the nucleus [11].

PDZK1-interacting protein 1 (PDZK1IP1), also known as MAP17, DD96, and SPAP, is a non-glycosylated membrane protein identified in the Golgi apparatus and plasma membranes [12, 13]. High levels of expression were detected in many types of human carcinomas [14, 15]. In particular, upregulation of PDZK1IP1 suppressed tumor necrosis factor-induced G1 arrest by downregulating p21 induction [14]. In addition, PDZK1IP1 reduces c-Myc-mediated caspase3-like activity in Rat1 fibroblasts in low serum, allowing them to keep the phosphatidylinositol 3-kinase/Akt signaling pathway active [16]. PDZK1IP1 overexpression in a colon cancer cell line inhibited cell growth in-vivo and in-vitro [12], and laryngeal carcinoma patients who have high PDZK1IP1 expression had longer laryngoesophageal dysfunction–free survival following treatment [17]. The decrease in expression of PDZK1IP1 has also been linked to tumorigenicity in lung adenocarcinoma [18]. In a xenograft nude mice model, NCI-H290 cells which showed enhanced cell proliferation in the presence of TGF- signaling, increased PDZK1IP1 expression suppresses tumorigenicity caused by TGF-β, While PDZK1IP1- deficiency resulted in substantially higher migratory efficiency compared to the control cell lines [19]. Moreover, PDZK1IP1 knockdown increased oral squama cell carcinoma (OSCC) migration and metastasis in-vitro and in-vivo. It was also shown that OSCC patients with high PDZK1IP1 expression in tumor tissues had a higher recurrence-free survival rate [20]. These results suggest that PDZK1IP1 may have a positive or negative role in tumorigenicity depending on the specific tumor being studied.

Atonal homolog 8 (ATOH8) is a novel transcription factor that belongs to the Net family in the atonal superfamily of the basic helix-loop-helix (bHLH) transcription factors [21]. ATOH8 regulates several developmental processes, including the nervous system, renal, pancreas, and muscular growth and development [22, 23]. bHLH transcription factors such as cMYC, Twist, and HIF-1 have been associated with tumor development and progression [24]; however, the role of ATOH8 in tumor growth remains unknown. Recent research has shown that ATOH8 deficiency promotes the stemness of hepatocellular cancer [25]. Another study found that ATOH8 downregulation led to the malignant phenotype of nasopharyngeal cancer [26], indicating that ATOH8 has a tumor-suppressive impact. In liver cancer cell lines, lower ATOH8 expression was related to increased CD133 positivity, while overexpressed ATOH8 inhibited cell growth, invasion, and migration. Most critically, by attaching to their E-Box sequences, ATOH8 depletion may reduce the activity of Oct4 and Nanog pluripotency regulators [26, 27]. They discovered that ATOH8 suppression directly released AFP, CD133, OCT4, and NANOG to reprogram non-cancer stem cells into cancer stem cells [27]. According to The Cancer Genome Atlas (TCGA), malignant tissues had significantly lower ATOH8 expression than matching peritumoral tissues in several malignancies, suggesting a role in carcinogenesis [27]. However, the precise function of ATOH8 in tumor metastasis and the underlying molecular mechanism are not well characterized.

Most importantly, the FXR1 expression level is significantly elevated in various malignancies. Its expression corresponds with poor outcomes among those affected with lung squamous cell carcinoma (LSCC), non-small cell lung cancer, ovarian cancer, breast cancer (BC), and head and neck squamous cell carcinoma (HNSCC) [28, 29]. Recent research has shown that the FXR1 expression level has elevated in colorectal cancer tissues and cells, facilitating cell proliferation, migration, and invasion [30]. Moreover, FXR1 is extensively expressed in OSCC tissues and cells, and it prevents cell senescence by binding to and enhancing the stability of non-coding RNA TERC [28]. In line with this, it was also shown that the overexpression of FXR1, CLAPM1, and EIF4G on amplicon 3q26-27 in LSCC was associated with the repressed immune response pathway [31]. Furthermore, HNSCC was revealed to be suppressed by FBXO4-mediated degradation of FXR1 [32]. Nonetheless, the function of FXR1-mediated regulation of gene expression in esophagus cancer (ESCA) and the underlying mechanism is poorly understood.

The present study demonstrates that FXR1 is considerably overexpressed in ESCA cell lines, suggesting that FXR1 may be implicated in ESCA development

by regulating the stability of *PDZK1IP1* and *ATOH8* mRNAs. Down-regulation of FXR1 significantly reduces the cell viability, proliferation and migration and promotes apoptosis, cell cycle arrest, and cellular senescence, hence preventing the progression of ESCA both in-vitro and in-vivo. Overexpression of PDZK1IP1 and ATOH8 reversed FXR1-induced effects on ESCA cell migration and proliferation. For the first time, our study highlights the importance of FXR1-*PDZK1IP1* and -*ATOH8* signaling in this disease, which might have potential diagnostic or therapeutic implications.

Materials and methods

Cell culture

The OE33 (FH1118-98), EC9706 (FH1118-112), EC109, and K450 human ESCA cell lines were obtained from Fenghbio Bio-sciences (Changsha, Hunan, China). The cells were cultured in RPMI1640 and DMEM medium supplemented with 10% fetal bovine serum, 100 µg/mL streptomycin, and 100 U/mL penicillin and were maintained at 37 °C in a humidified environment of 5% CO2 and 95% air.

Plasmid construction

Overexpression and knockdown of FXR1 were performed using plasmids packaged into lentivirus provided by (OBiO Technology (Shanghai) Corp., Ltd.). Negative controls in our experiments comprised cells transfected with a scrambled siRNA sequence provided by the company. Cells were infected with lentiviruses for overexpression and knockdown at a multiplicity of infection (MOI) of 0.5 and then screened with 3 µg/ml puromycin. The coding sequence (CDS) of human *PDZK1IP1* (NM_005764.4) was cloned into the pcDNA3.1 (+) vector (Invitrogen) to generate the PDZK1IP1 overexpression construct. To generate a construct overexpressing ATOH8, the CDS of human *ATOH8* (NM_032827.7) was cloned into the pcDNA3.1 (+) vector. We used the lipofectamine 8 Transfection Reagent (Shanghai Yuanye Bio-Technology Co., Ltd) to transfect the plasmid and the control vector into cells at 100 nmol/L concentration. The transfection efficacy was assessed by qRT-PCR or Western blotting.

Cell viability assay

Cell viability was detected using a Cell Counting Kit-8 (CCK-8) (COOLBER Science & Technology) assay. Following transfection, cells were seeded in 96-well plate at a density of 1000 cells per well. After 24 h, 10 µl of CCK-8 solution was added to each well, and the plates were incubated for 2 h at 37 °C. A microplate reader was used to measure the absorbance at 450 nm with the automatic microplate reader (Clarion Star Plus). OD with five repetitions of each group was determined to check the cell viability.

Cell proliferation assay

The Light EdU Apollo 567 in Vitro Imaging Kit (RiboBio, Guangzhou, Guangdong, China) was used to analyze cell proliferation. Briefly, a 96-well plate was seeded with 1.2×10^4 cells/well and incubated for 24 h. After removing the growth media, EdU A-containing pure growth medium was added and incubated for 2 h. Following a wash in PBS, cells were fixed with 4% paraformaldehyde (PFA). By adhering to the kit protocol, the Apollo procedure was performed in dark conditions. After being washed with PBS and methanol, cells were stained with Hoechst reagent at room temperature and in the dark. After the imaging step using a fluorescent microscope, the proliferation rate was determined using the following formula: Proliferation percentage = (EdU positive cells/total cells) x 100.

Colony formation assay

To examine the effect of FXR1 differential expression on colony formation, cells were seeded in triplicates (2.4×10^3) on a 6-well plate and cultured for one week at 37 °C in a 5% CO2 incubator. After one week, cells were thoroughly washed with PBS and fixed with methanol at room temperature. The cells were then stained with 0.2% crystal violet and allowed to incubate at room temperature. The colonies were then identified by scanning the plate.

Wound healing assay

The scratch wound-healing motility assay was applied to assess the migrating ability of FXR1 knockdown/overexpression-treated ESCA cell lines. The cells were scraped over a monolayer using a sterile pipette tip when they were 80–90% confluent on a 6-well plate. A light microscope was used to monitor the migration rate at 0 h, 24 h, and 48 h. The width was calculated using Image J software to measure the migration rate. The migration rate (MR) was calculated as MR (%) = [(A0 - A1)/A0] 100, where A0 and A1 are the widths at 24 h and 48 h, respectively.

Migration assay

To measure the FXR1 knockdown/overexpression-treated cell migration, we dropped 200 µl of medium and cell suspension in the upper chamber of a 24-well plate. As a chemoattractant, 20% fetal bovine serum (600 µl of medium) was placed in the bottom chamber. Following a 24-hour incubation period, cells were fixed with methanol for 20 min before being stained for 40 min with a crystal violet dye solution. Subsequently, transwell migration images were obtained using a Zeiss Axioskop 2 plus microscope (Carl Zeiss, Thornwood, NY, USA).

The apoptotic marker annexin V-APC/7AAD staining

Following the manufacturer's instructions, cell apoptosis was determined using an Annexin V-APC/7AAD Apoptosis Detection Kit I (Lianke bio). Cells were seeded in 6 wells plate and grown until the confluency reached > 90%. Following 48 h, the cells were trypsinized, washed with PBS, and resuspended in Annexin V binding buffer. V-APC and 7-AAD were added to each tube, mixed, and incubated for 5 min in the dark at room temperature. Samples were analyzed through a flow cytometry machine (Beckman colter), and data was obtained using MFLT32 software (TreeStar, Ashland, OR, USA).

Cell cycle analysis

Following the FXR1 knockdown/overexpression, flow cytometry was used to determine the percentage of cells in each phase of the cell cycle. In 6-well plate, cells were seeded until confluence reached > 90%. Cells were washed with PBS, digested with trypsin, and collected in tubes. Each tube was pre-mixed with the DNA staining solution (A) and the permeabilization solution (B) and incubated in the dark for 30 min at room temperature. Then, the cell cycle rate was evaluated using flow cytometry.

Western blot analysis

The cells were lysed in RIPA lysis buffer, including the complete protease inhibitor cocktail (Abcam, ab271306). Protein concentration was determined using a BCA reagent (Thermo Scientific, Cat#23225). An equal amount of each protein sample was separated by electrophoresis in 10% sodium dodecyl sulfate-polyacrylamide gels and followed by transferring to a polyvinylidene fluoride membrane on ice. Then, 5% fat-free milk powder in TBS with 0.1% Tween-20 (Sigma-Aldrich; Merck, Germany) was used to block the PVDF membranes for 1 h. The protein blots were hybridized overnight at 4 °C with the appropriate primary antibodies. The internal control was chosen to be β-actin. After incubation with secondary antibodies, the protein bands were visualized using the enhanced chemiluminescence technique (ECL, Millipore, MA, USA). All antibodies used for this research are listed in Table S1.

RNA immunoprecipitation (RNA-IP) assay

Following the manufacturer's instructions, the RNA-IP assay was carried out using the Magna RIP RNA-Binding Protein Immunoprecipitation Kit (MilliporeSigma, Burlington, MA, USA). After whole-cell protein extraction from OE33 cells, the lysates were treated for 4 h at 4 °C with the corresponding antibodies coupled to Dynabeads Protein A/G. Following thorough washing, the immobilized immunoprecipitated complexes were incubated with proteinase K for 30 min at 55 °C to break down the protein. The co-precipitated RNA was eluted and purified using Trizol Reagent before being tested by PCR. The primer sequences for the genes selected for RNA-IP are listed in Table S2.

RNA extraction and quantitative real-time PCR (qRT-PCR)

Total RNA was isolated from cells using Trizol reagent (Life Technologies Corporation, Carlsbad, CA). RNA concentration was measured at 260/280 nm using a nanodrop Spectrophotometer (ND-100, Thermo, Waltham, MA). The qRT-PCR was utilized to identify *FXR1*, *PDZK1IP1*, *ATOH8*, and *GAPDH* using the One-Step SYBR PrimeScript RT-PCR Kit from (Takara Bio, Inc., Japan).

RNA stability measurement

After transfected with sh-NC or sh-FXR1, 5 μg/ml Actinomycin D (ActD; Cell Signaling, 10 μg/ml) was added to block FXR1 transcription. Total RNA was collected at indicated times (3 h, 6 h, 12 h), and *PDZK1IP1* and *ATOH8* expression were measured by qRT-PCR. The half-life of *PDZK1IP1* and *ATOH8* was determined as the time required to reach 50% of the RNA levels before adding Actinomycin D.

Animal experiments

The animal study was approved by the Henan University School of Medicine's Committee on Medical Ethics and Welfare for Experimental Animals (HUSOM-2019-168). Animal experiments were conducted similarly to those reported in [33], with minor modifications. The BALB/C nude mice (male, 4 weeks old) were supplied by Vital River Laboratory Animal Technology Co., Ltd. (Beijing, China). The right flanks of null mice were subcutaneously injected with OE33 and EC9706 (5×10^6 cells in 200 μl PBS. The mice were randomly assigned into four groups ($n=5$ each). For 28 days, 10 mM FXR1-KD, FXR1-KD + PDZK1IP1-OE, and FXR1-KD + ATOH8-OE were administered subcutaneously near the tumor. PBS was administered subcutaneously to the control animals. The tumor volumes and body weights were recorded daily. We used the following formula to determine the tumor volume: volume = length x width 2/2. The mice had a general anesthetic at the end of the trial with 3% isoflurane, which was executed by dislocating the cervical region. To determine the rate at which tumor development was inhibited, we used the formula IR (%) = [(A B)/A] 100, where A and B are the mean tumor weights for the control and treatment groups, respectively.

Tumor tissue staining

Tissues were sectioned to a thickness of 5 mm and stained with hematoxylin and eosin (HE) after being preserved in paraffin-embedded in 10% neutral-buffered

formalin. The images were captured using a Zeiss Axioskop 2 plus microscope.

Immunohistochemistry (IHC)

The tumor microvessel density (MVD) was calculated using the Cluster of Differentiation 31 (CD31), an effective biomarker for vascular endothelial cells [34]. The CD31 antibody (CST) was used to stain tissues, and a Zeiss Axioskop 2 plus microscope was used to identify and quantify tumor vascular density. Additionally, an anti-Ki67 antibody (CST) was used to stain the tumor tissues, and a Zeiss Axioskop 2 plus microscope was used to take pictures of the Ki67 antibodies and positive cells. To determine the proliferation index (PI), we divided the number of Ki67-positive cells by the total cell count [35]. Similarly, the apoptotic index (PI) was determined by staining tumor samples with an antibody against cleaved caspase-3. The percentage of cells that had been cleaved caspase-3 compared to the total number of cells was used to determine the cell death rate [36].

Statistics analysis

All experimental results were presented as the mean standard error of the mean (SEM). When comparing the two groups, we employed the two-tailed Student's t-test to determine significant variation. Using the GraphPad Prism 7 (GraphPad, San Diego, CA) statistical analysis program, a one-way analysis of variance and Tukey's test were used to determine variation between the various groups. $P<0.05$ was considered to be statistically significant.

Results

FXR1 is upregulated in ESCA cell lines

Utilizing the Timer2 database (http://timer.cistrome.org/), we found that FXR1 expression was higher in ESCA and several other cancer types compared to adjacent normal tissue samples from the TCGA dataset (Fig. 1A). To further investigate the role of FXR1 in ESCA oncogenesis, we conducted a high-resolution SNP-based copy number analysis on 185 ESCA patients from the TCGA datasets, identifying potential oncogenes at 3q26. Our

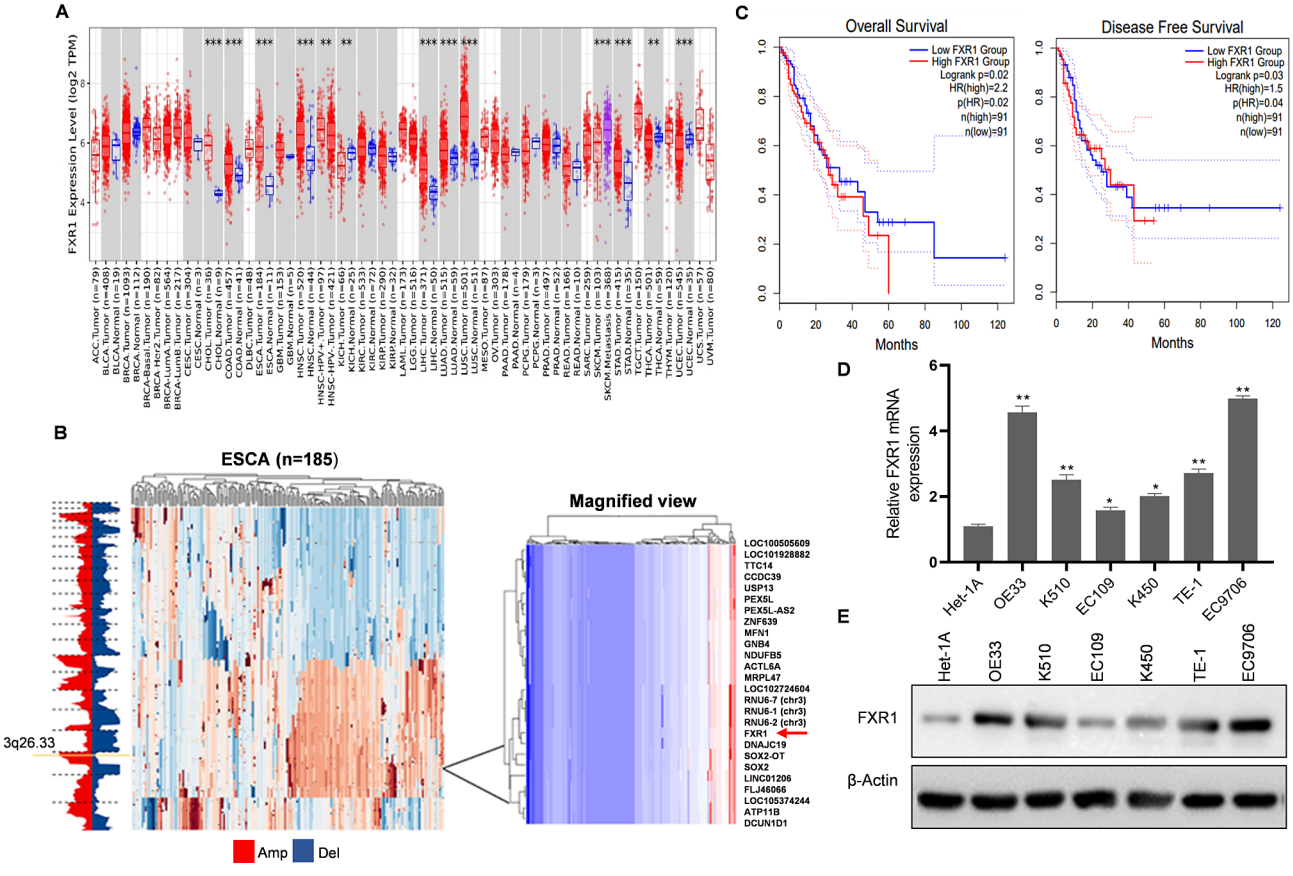

Fig. 1 *FXR1* mRNA and protein associated with the progression of ESCA. (**A**) FXR1 differential expression between tumor vs. adjacent normal tissues in different cancers. (**B**) Heatmap of chromosome 3q26.3 locus amplification in the dataset of 185 patients with ESCA from the TCGA dataset. (**C**) In 182 patients with ESCA, the Kaplan-Meier plot shows the FXR1 expression-based result of overall survival and recurrence-free survival. A log-rank test was used to determine the p-value. (**D**) *FXR1* mRNA expression quantification analysis in ESCA cells by qRT-PCR. (**E**) FXR1 protein expression levels in normal human esophagus cells and ESCA cells. β-actin is used as a loading control

analysis revealed that FXR1 is significantly amplified or shows elevated copy numbers in approximately 40% of ESCA patients (Fig. 1B). Although various mutations are present in FXR1, amplification was the most common mutation across all cancer types and was linked to poorer overall survival. Our data indicate that increases in *FXR1* mRNA and protein levels are associated with gene copy number amplification. Higher *FXR1* mRNA expression correlates with poorer overall survival and recurrence-free survival in ESCA patients, suggesting that high FXR1 expression is a marker of poor prognosis. Further analysis using the UALCAN portal confirmed that FXR1 is frequently amplified in several other malignancies, including lung, ESCA, ovarian, cervical, HNSCC, and uterine carcinomas. Notably, high-grade ESCA and advanced tumors exhibited significantly higher FXR1 protein levels (Fig. S1A, B, C). Additionally, FXR1 overexpression was associated with a significant increase in disease-related mortality, with a hazard ratio of 2.2. These findings suggest that FXR1 overexpression plays a critical role in cancer progression (Fig. 1C).

We then compared *FXR1* transcript and protein levels in ESCA cell lines. Total RNA and protein were isolated from Het-1 A, OE33, K510, EC109, K450, TE-1, and EC9706 cells, respectively. The mRNA levels of *FXR1* in these cell lines were measured using qRT-PCR. *FXR1* transcripts were found to be considerably higher in all ESCA cells than in normal esophageal cells, as shown in Fig. 1D. The highest expression was observed in the OE33, K510, TE-1, and EC9706 cells, which were selected for FXR1 knockdown investigations. For FXR1 overexpression studies, the EC109 and K450 cell lines were selected because of their lower FXR1 expression. Consistently, the FXR1 protein detected by Western blotting exhibited identical results in malignant cells compared to normal counterparts (Fig. 1E). According to our findings, FXR1 was overexpressed in ESCA cells.

FXR1-silencing reduces ESCA cell proliferation and viability

Next, we administered shRNAs to inhibit FXR1 expression in OE33 cells precisely. The efficacy of the knockdown was validated by Western blotting, as shown in Fig. 2A. The potential effect of FXR1 knockdown on cell proliferation and viability of ESCA cells was investigated using CCK-8, colony formation, and EdU assay. As depicted in Fig. 2B, C, the cell viability and proliferation of FXR1-deficient cells was substantially impaired compared to wild-type cells. Additionally, we stably over-expressed FXR1 in EC109 and K450 cell lines, both of which showed a low level of endogenous FXR1 expression (Fig. 2A). Overexpression of FXR1 markedly increases cell viability and growth as determined by CCK-8, colony formation, and the EdU assay (Fig. 2D, E, S2), thus encouraging cancer progression. The findings indicated that FXR1 knockdown significantly decreased cell viability and proliferation in OE33 cells.

FXR1-silencing reduces ESCA cell migration

We next determined whether FXR1 had any effect on the aggressive behavior of ESCA cells in terms of their ability to migrate and invade new tissues. Therefore, we evaluated FXR1 expression using transwell and scratch assays. As shown in Fig. 3A and B, FXR1-deficient OE33 cells displayed markedly reduced migration. Additionally, a comparable result was observed when FXR1 was overexpressed in EC109 and K450 cells (Fig. 3C, S3). Our findings suggested that in addition to cell proliferation, FXR1 played essential roles in the malignant behavior of ESCA cells.

FXR1-silencing induces apoptosis in ESCA cells

Evasion of cell death is one of the critical modification that happen when a normal cell transforms into a malignant cell, and this transformation causes carcinogenesis. Therefore, a reduction in apoptosis or resistance to apoptosis plays a crucial role in cancer progression. Annexin V-APC/7-AAD staining was performed to determine whether FXR1 drives ESCA cell apoptosis. Compared to the sh-NC control group, the FXR1 knockdown cells displayed considerably greater percentages of early and late apoptotic cells. According to the findings of the apoptosis detection experiment, FXR1 knockdown increased the rates of early and late apoptosis in ESCA cells (Fig. 4A). On the contrary, FXR1 overexpression prevents the apoptosis of EC109 ESCA cells, further supporting the notion (Fig. 4B). The apoptosis-related signaling pathways were similarly modified by FXR1 inhibition. Proapoptotic proteins, such as cleaved-PARP, cleaved-Caspase3, and Bax were upregulated in FXR1-deficient cells, whereas antiapoptotic Bcl-2 levels were downregulated (Fig. 4C). Hence, our findings imply that FXR1 may facilitate ESCA cells' escape from the regular cell death process.

FXR1 knockdown triggers cell cycle arrest in ESCA cells

To study the mechanism of cell proliferation and migration, we employed flow cytometry to investigate the number of cells in various cell cycle phases in FXR1 Knockdown/overexpression and control cells. The Knockdown of FXR1 in OE33 cells results in G0/G1 cell cycle arrest (Fig. 4D), suggesting that FXR1 regulates cell division in ESCA. As shown in Fig. 4E, our findings provided additional evidence that overexpression of FXR1 suppresses the cell cycle arrest in the G0/G1 phase. Altogether, our results showed that FXR1 depletion caused cell cycle arrest in ESCA cells' G0/G1 phase, supporting its involvement in cell division regulation.

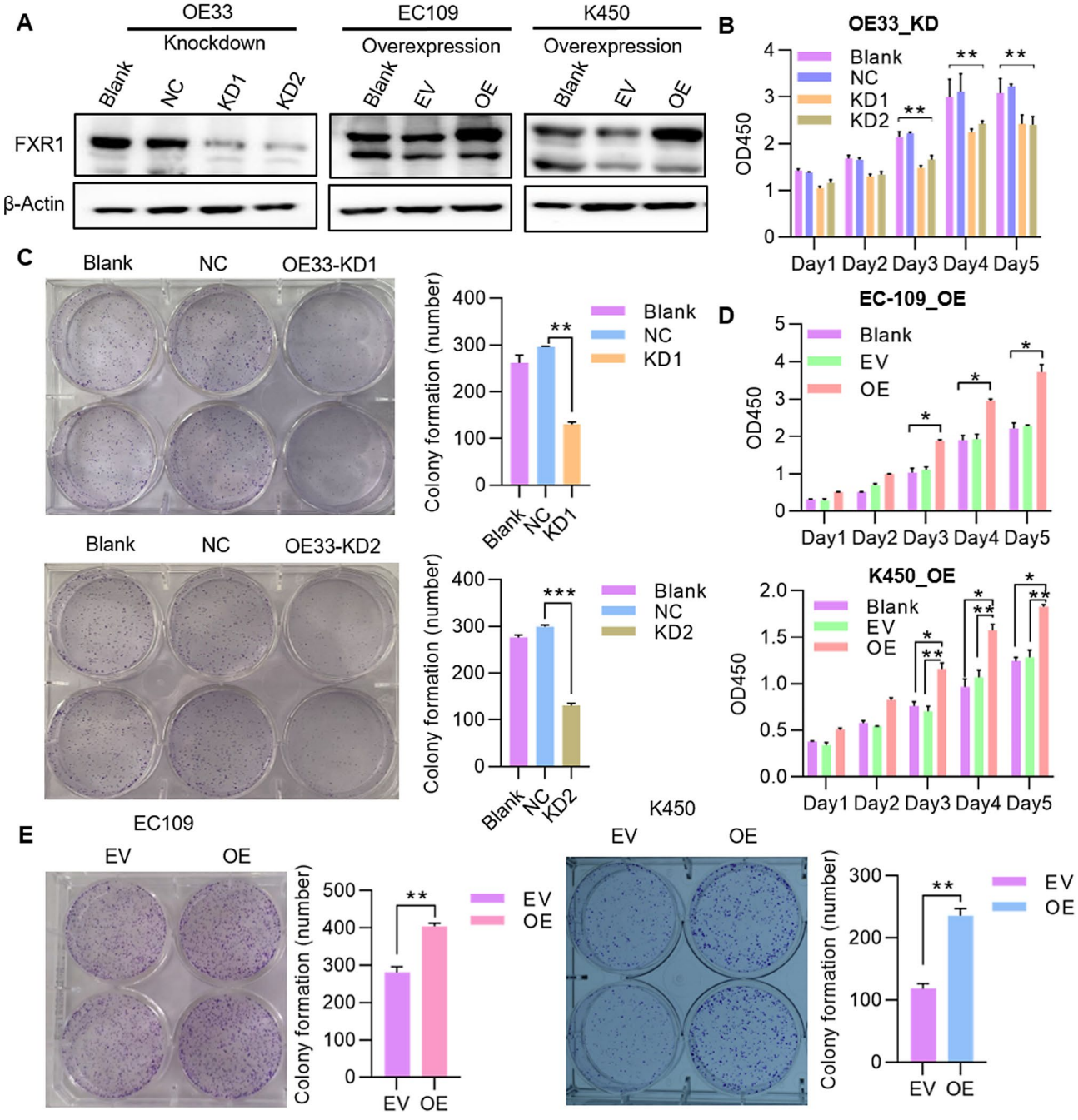

Fig. 2 FXR1 knockdown inhibited the proliferation of ESCA cells. (**A**) ESCA cells were transduced with lentivirus that express two different shRNAs targets FXR1 (KD1 and KD2), control shRNA (NC), or orf (OE) along with empty vector (EV), and western blot was performed 72 h after transduction using antibodies indicated. β-actin is used as a loading control. (**B**) ESCA cells were transduced using the FXR1 shRNAs, and cell viability was determined using the CCK-8 assay at indicated time points. Each experiment was performed for 5 days and in triplicates. (**C**) ESCA cells were transduced using the FXR1 shRNAs and subjected to a 6–8 days' colony formation assay. The number of colonies was calculated. (**D**) ESCA cells were transduced using the FXR1 orf (OE), and cell viability was determined using the CCK-8 assay at indicated time points. Each experiment was performed for 5 days and in triplicates. (**E**) ESCA cells were transduced using the FXR1 orf (OE) and subjected to a 6–8 days colony formation assay. The number of colonies was calculated. Scale bar, 100 mm. Data are presented as the mean ± SEM ($n = 3$ in each group). $^{*}P < 0.05$, $^{**}P < 0.01$

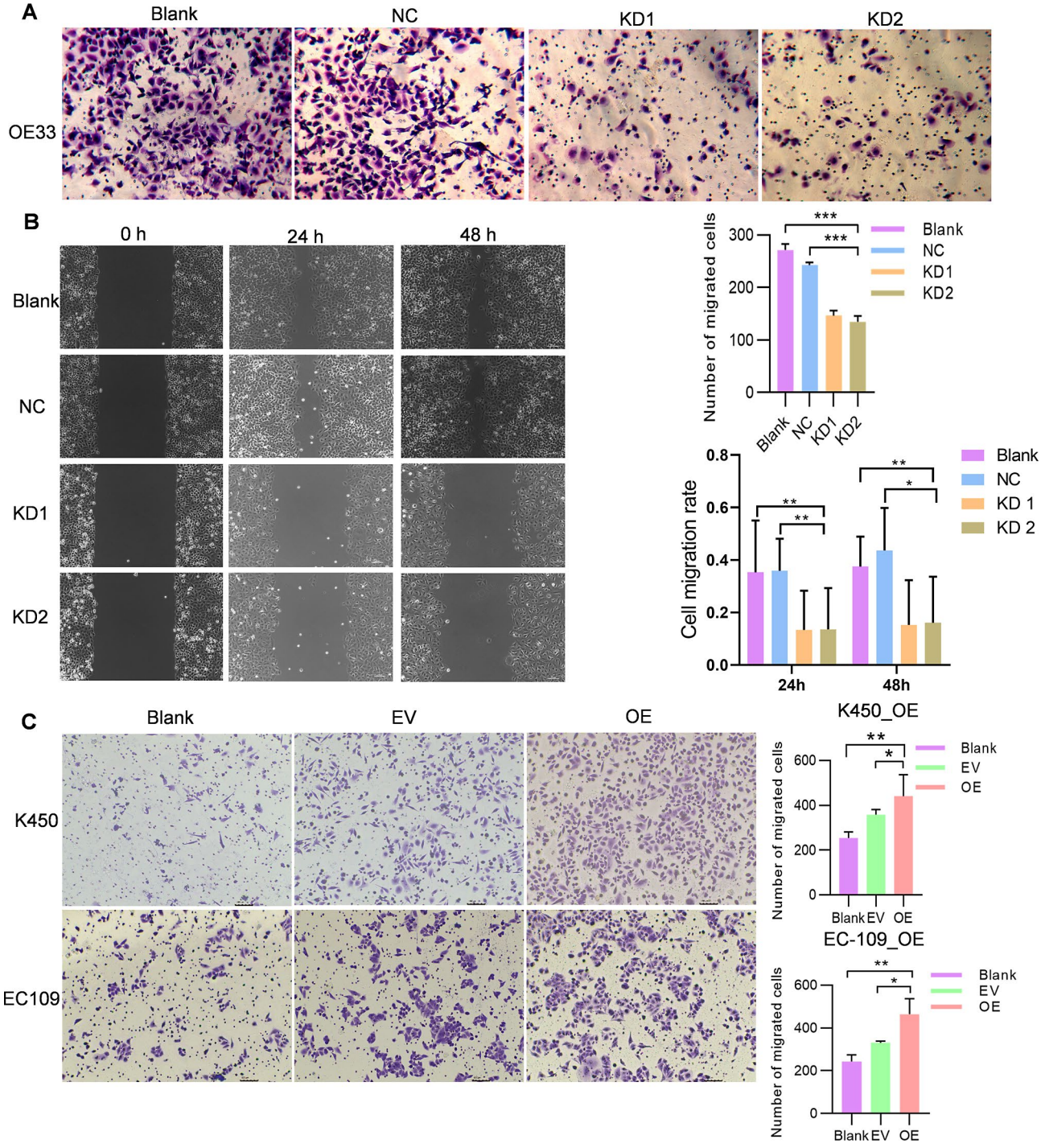

Fig. 3 FXR1 knockdown inhibited the migration of ESCA cells. (**A**) OE33 cells were transduced with shNC, and shRNAs target FXR1 (KD1 and KD2) followed by Transwell assay for cell migration. The cells were then observed microscopically (magnification, x200). The relative images and accompanying statistical plots were presented. The experiments were performed in triplicate. (**B**) Cell migration was measured by scratch assay (original magnification × 100). The number of migrated cells was calculated. (**C**) K450, EC109 cells were transduced with FXR1 orf (OE) followed by Transwell assay for cell migration. The cells were then observed microscopically (magnification, x200). The relative images and accompanying statistical plots were presented. The experiments were performed in triplicate. Data are presented as the mean ± SEM ($n = 3$ in each group). *$P < 0.05$, **$P < 0.01$. Note: The difference in cell status and the time of spreading the plates resulted in inconsistencies in the number of cells in the control group at different times

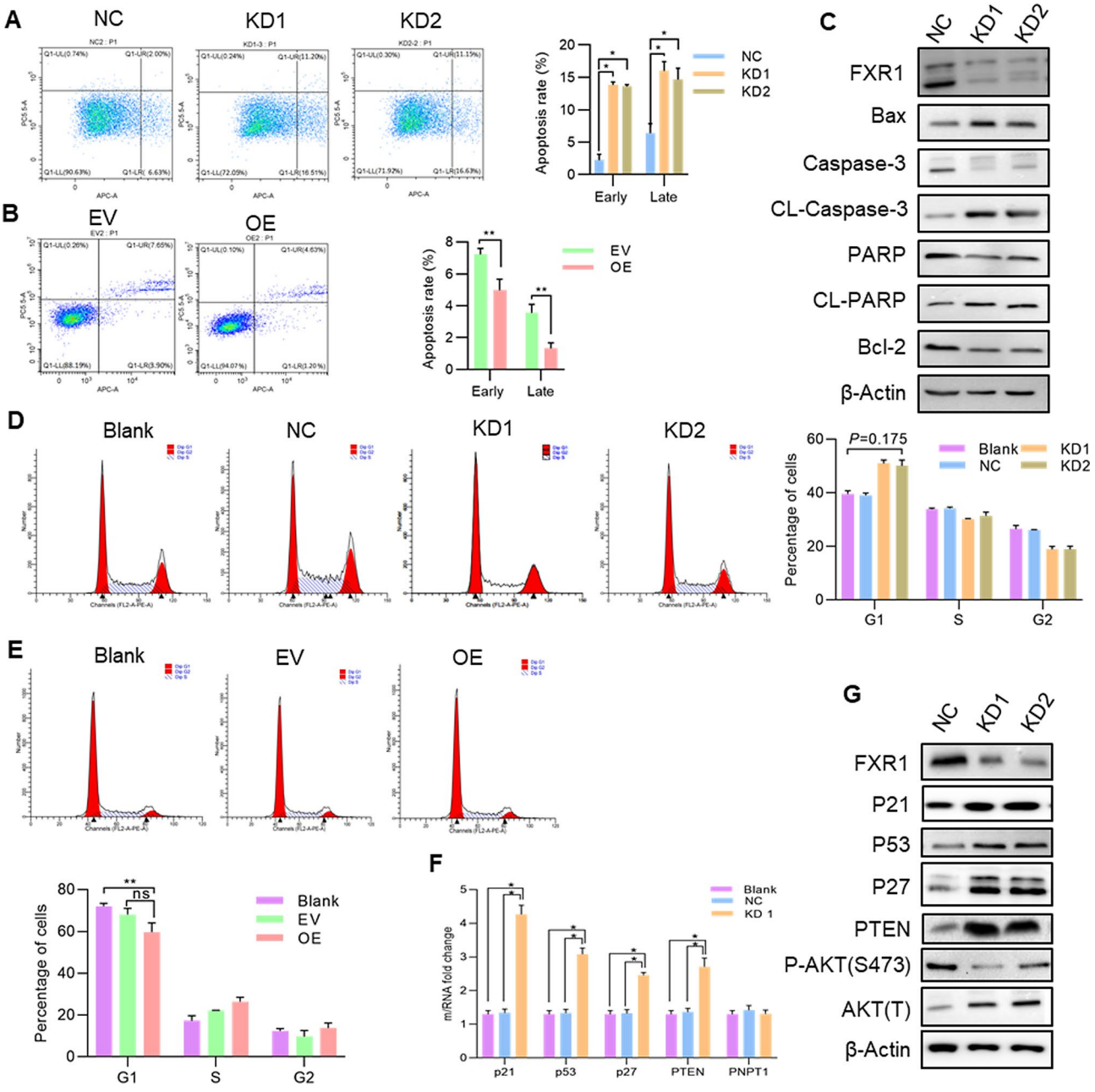

Fig. 4 FXR1 knockdown inhibited the growth of ESCA cells by promoting apoptosis. (**A**) Cells transduced with FXR1 shRNAs (KD1, KD2) or (**B**) FXR1 orf (OE) and then subjected to flow cytometric analysis to evaluate the effect of FXR1 knockdown or overexpression on the apoptosis of OE33 cells. (**C**) Western blot analysis shows the expression pattern of apoptosis-related proteins in FXR1 knockdown cells. (**D**) Cell transduced with FXR1 shRNAs were then processed for cell cycle experiment and analyzed by flow cytometry. (**E**) Cell transduced with FXR1 overexpression (OE) were then processed for cell cycle experiment and analyzed by flow cytometry. (**F**) The relative quantity of the senescence protein-coding RNAs extracted from control and FXR1-depleted cells is estimated by using qRT-PCR. β-actin serves as a control. (**G**) Immunoblot analysis of senescence marker proteins in FXR1 depleted cells. β-actin is used as a loading control. The experiments were performed in triplicates. Data are presented as the mean ± SEM ($n = 3$ in each group). *$P < 0.05$, **$P < 0.01$

FXR1 knockdown promotes cellular senescence in ESCA cells

Cellular senescence is characterized by several features, one of which is an arrest of the cell cycle. We assessed the expression of genes for senescence markers to ascertain if FXR1 regulates cellular senescence by altering post-transcriptional gene expression. As shown in Fig. 4F, the reduction of FXR1 increased *p21*, *p27*, *p53*, and *PTEN* mRNA levels in OE33 cells. Following FXR1 knockdown, protein levels of p53, PTEN, p21, and p27 increased in OE33 cells, validating our results (Fig. 4G). In addition, FXR1 knockdown OE33

cells had lower levels of pAkt (Ser-473) than control and total Akt, demonstrating that FXR1 may regulate cellular senescence via inhibiting the phosphatidylinositol 3 kinase/Akt signaling pathway.

FXR1-silencing increases PDZK1IP1 and ATOH8 level

The next step was to find a putative downstream effector of FXR1. Based on RNA-IP results, we found that the mRNA of *PDZK1IP1* and *ATOH8* genes was enriched in the FXR1 immunoprecipitated RNA complexes (Fig. 5A). To comprehend better the underlying regulatory mechanism, the stability of *PDZK1IP1* and *ATOH8* transcripts was examined in response to FXR1 knockdown or overexpression. Knockdown of FXR1 stabilized *PDZK1IP1* and *ATOH8* transcripts in OE33 cells. We found that *PDZK1IP1* and *ATOH8* mRNA levels were considerably higher in FXR1-deficient cells than in scrambled controls (Fig. 5B), suggesting that these proteins may promote the FXR1 oncogenic role in ESCA. We further investigated the transcript level of these genes in FXR1 overexpressed EC109 and K450 cells and discovered that *PDZK1IP1* and *ATOH8* transcription was significantly down-regulated upon FXR1 overexpression (Fig. 5C), indicating that FXR1 modulated *PDZK1IP1* and *ATOH8* expression at the transcription level. In FXR1-deficient cells, *PDZK1IP1* and *ATOH8* mRNA levels increased by 60% and 30%, respectively. In contrast, their expression decreased by 56.5% and 48% when FXR1 was overexpressed, compared to scrambled controls. Therefore, our findings showed that FXR1 inhibited *PDZK1IP1* and *ATOH8* expression by accelerating the FXR1 transcript decay mechanism.

FXR1 regulates PDZK1IP1 and ATOH8 expression through 3′ UTR

The full-length *PDZK1IP1* and *ATOH8* mRNA are used for RBP binding site prediction using RBPsuite (http://www.csbio.sjtu.edu.cn/bioinf/RBPsuite/). As shown in Fig. 5D, *PDZK1IP1* and *ATOH8* had two and three FXR1 binding sites, respectively, that were independently identified in the CLIP-seq peaks and verified on segments with known binding sites. The conserved sequence motif of the FXR1 protein is shown in Fig. 5E. To give further support evidence for anticipated binding sites, we employed RBPmap (http://rbpmap.technion.ac.il/) to corroborate the observed binding sites (Fig. 5F). These results complement our previous findings that FXR1 controls *PDZK1IP1* and *ATOH8* expression post-transcriptionally via interactions with particular binding sites.

PDZK1IP1 rescues the phenotype induced by FXR1

To elucidate the specific regulatory function of PDZK1IP1 in mediating FXR1 oncogenic role in ESCA cells, we conducted experiments where PDZK1IP1 was overexpressed independently or in conjunction with FXR1-overexpressed EC109 cell lines and analyzed the corresponding phenotypes, including cell viability, proliferation, and migration. As depicted, FXR1-overexpression stimulates cancer cell viability, PDZK1IP1 overexpression- either alone or in FXR1-overexpressed cells mitigated these effects in EC109 cells (Fig. 6A). Similarly, colony formation assay demonstrated a significant restoration of cell proliferation in PDZK1IP1-overexpressing cells, either alone or in combination with FXR1, compared to cells overexpressing FXR1 alone (Fig. 6B). Furthermore, malignant behaviors such as migration, which were considerably compromised in FXR1-overexpressed cells, were completely revered by PDZK1IP1 overexpression (Fig. 6C). The previous finding indicates that FXR1 deficient cells had lower levels of expression of EMT-related proteins as well as SMAD2/3. Consistent with this, PDZK1IP1 overexpression in EC109 cells led to decreased levels of mesenchymal markers such as SLUG, N-cadherin, vimentin, Snail-2, Zeb-1, and SMAD2/3, compared to control cells (Fig. 6D). These findings suggest that FXR1 may regulate the expression of EMT-related proteins through the PDZK1IP1 pathway.

Analysis of transcriptome sequencing data from 179 ESCA samples obtained from the GEO database, combined with multivariate Cox analysis, identified PDZK1IP1 as an independent risk factor for overall survival, with higher expression associated with a better prognosis ($p=0.031$). A violin plot showed significantly higher PDZK1IP1 expression in normal tissues compared to cancerous ones ($p<0.001$) (Fig. S4A, B). Our analysis also revealed a negative correlation between the mRNA expression levels of FXR1 and PDZK1IP1, indicating that FXR1 acts as a negative regulator of PDZK1IP1 gene expression (Fig. S4C). This interaction was further validated through STRING protein interaction network analysis and GeneMANIA, which confirmed strong connectivity between PDZK1IP1 and FXR1 (Fig. S5A, B). These results suggest that overexpression of PDZK1IP1 could be effective strategy for inhibiting FXR1-induced cancer metastasis in human.

ATOH8 rescues the proliferation abundance in FXR1

Decreased FXR1 expression results in elevated levels of several tumor-suppressive proteins, including ATOH8. To investigate whether ATOH8 acts as an essential regulator of FXR1, we assessed the impact of increasing ATOH8 levels on FXR1-induced cancer cell viability, proliferation, and migration. To demonstrate that FXR1 effects were mediated via ATOH8, we restored ATOH8 in FXR1-overexpressing cells using *ATOH8* CDS lacking the 3′UTR and discovered that *ATOH8* restoration mitigated the increase in cell viability and colony formation induced by FXR1-overexpression (Fig. 7A,

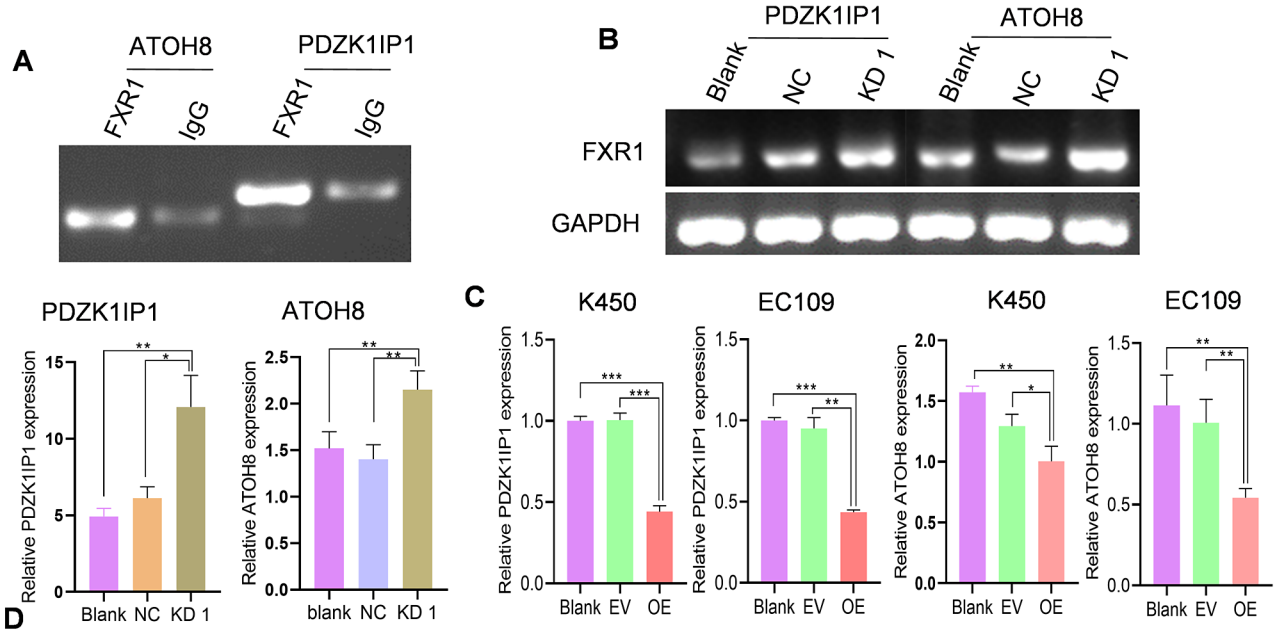

D

Sequence name	Sequence	Score
PDZK1IP1_motif 1	GCCAUGUCGGCCCUCAGCCUCCUCAUUCUGGGCCUGCUCACGGCAGUGCCACCUGCC AGCUGUCAGCAAGGCCUGGGGAACCUUCAGCCCUGGAUGCAGGG	0.530119
PDZK1IP1_motif 2	CCGUCGGAAACAAGGCAGAUGGAGUCCUGGUGGGAACAGAUGGAAGGUACUCUUCGA UGGCGGCCAGUUUCAGGUCCAGUGAGCAUGAGAAUGCCUAUGAG	0.6568217
ATOH8_motif 1	UCCUGAGGAACUUGAUAGACAAACAAUGACAGUGUUUUCCAGAACUGUGGGUACGUGU CUAAUCUCAGAUGGUACUAUGAAUUCCUGGAGAUCAAAGUUUG	0.9388821
ATOH8_motif 2	UCAAGGAGACCCUCAGCAAAAUAUAAAUGACGAGGAGCUGCCCUCAUGGGGCCCUGUG AAAGCACUUUGCAGUCCAGCCUUGGGUUUGUGGUCACAGAGU	0.936801
ATOH8_motif 3	GACCAGCUGCCUGUCAGACACUAAGAUAGGCAGUGGGAAUGAAGAGAUGGAUCUUGUG UCAUGCAUGGCAUCACGGAGCUCUGGGUUCUGUACGGAGGGUG	0.5166229

E

F

PDZK1IP1				
Sequence Position	FXR1-Motif	K-mer	Z-score	P-value
387	Aygacr	Caugag	1.900	2.87e-02
ATOH8				
Sequence Position	FXR1-Motif	K-mer	Z-score	P-value
4370	Aygacr	aaugac	3.043	1.17e-03
5479	Aygacr	aaugac	2.086	1.85e-02

Fig. 5 FXR1 bind to *PDZK1IP1* or *ATOH8* and regulate their expression post-transcriptionally. (**A**) RNA-IP assay was carried out using a monoclonal antibody specific for FXR1 to confirm the direct binding of FXR1 with *PDZK1IP1* or *ATOH8* mRNAs. Total RNA was extracted, and PCR was performed to investigate the enrichment of specific mRNA from the pulldown complex. (**B**, **C**) *PDZK1IP1* or *ATOH8* gene expressions were validated by qRT-PCR in FXR1 knockdown or overexpression cells. (**D**, **F**) The predicted binding regions of FXR1 on *PDZK1IP1* and *ATOH8* mRNAs. **E**) Conserved sequence motif of the FXR1 protein. Data are presented as the mean ± SEM ($n = 3$ in each group). $^{*}P < 0.05$, $^{**}P < 0.01$

B). Additionally, ATOH8 overexpression reversed the malignant behaviors, such as migration, that were significantly enhanced by FXR1 overexpression (Fig. 7C). Further analysis revealed that ATOH8 overexpression led to a significant decrease in the expression of mesenchymal markers β-catenin, vimentin, and N-cadherin, while increasing the expression of the epithelial marker E-cadherin (Fig. 7D).

We observed that ATOH8 expression was reduced in various cancer types, including ESCA, compared to adjacent normal tissue samples from the TCGA dataset (369 ESCA patients and 160 control). The results showed a significant twofold reduction in ATOH8 expression in

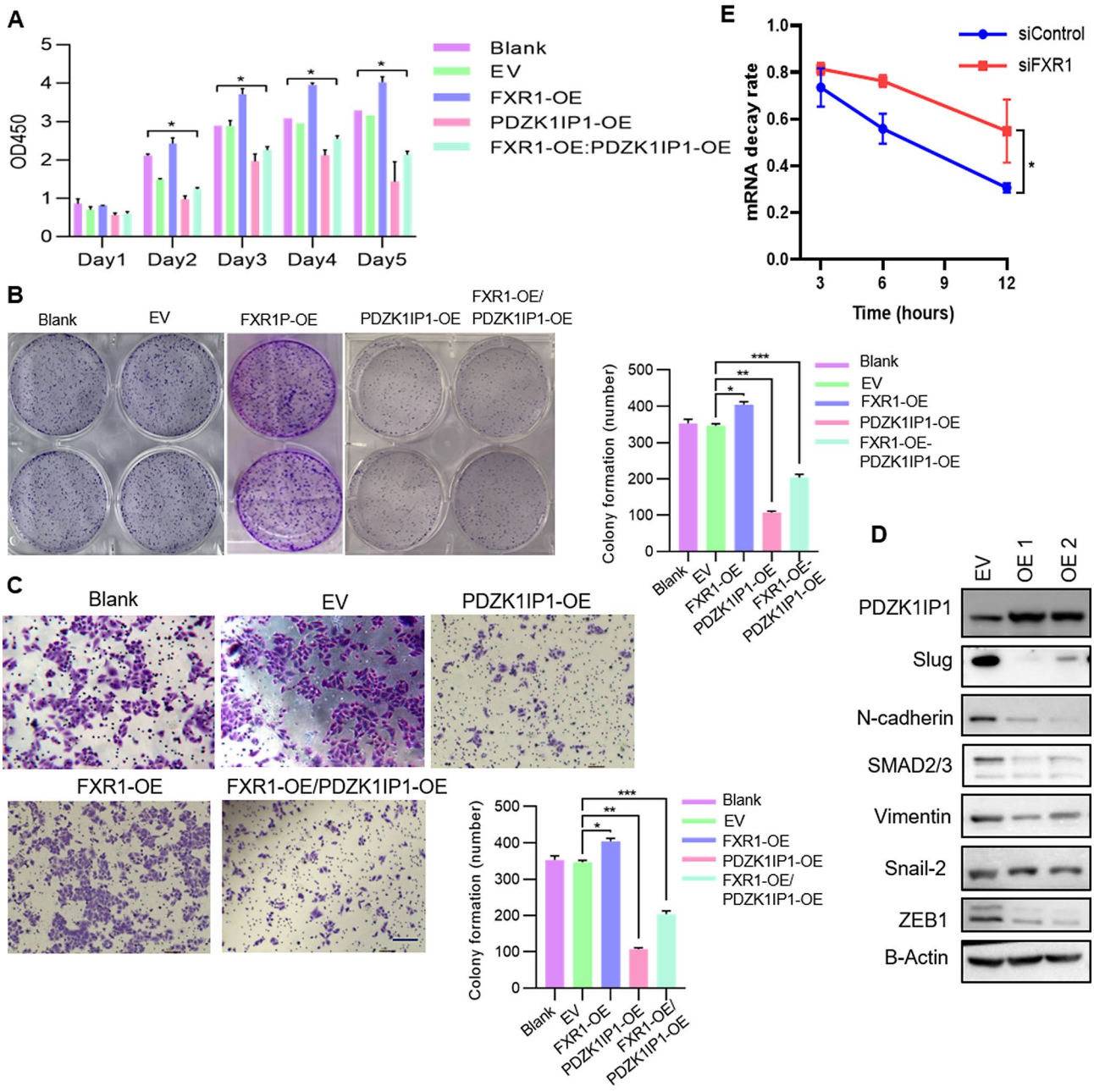

Fig. 6 PDZK1IP1 overexpression inhibited the proliferation and migration of ESCA cells. (**A**) ESCA cells were transfected using the PDZK1IP1 overexpression, and cell viability was determined using the CCK-8 assay at indicated time points. Each experiment was performed for 5 days and in triplicates. (**B**) ESCA cells were transfected using the PDZK1IP1 overexpression and subjected to a 6–8 days colony formation assay. The number of colonies was calculated. Scale bar, 100 mm. (**C**) ESCA cells were transfected with PDZK1IP1 overexpression followed by Transwell assay for cell migration. The cells were then observed microscopically (magnification, x200). The relative images and accompanying statistical plots were presented. The experiments were performed in triplicate. (**D**) Western blot detected EMT-related proteins' expression levels in PDZK1IP1 overexpressed cells. β-actin is used as a loading control. (**E**) qRT-PCR analysis revealed the half-life of *PDZK1IP1* mRNA in control or FXR1 knockdown cells after treatment with Actinomycin D. Data are presented as the mean ± SEM ($n = 3$ in each group). $^{*}P < 0.05$, $^{**}P < 0.01$

ESCA tumor tissue compared to normal tissue ($P<0.05$) (Fig. S6A). Furthermore, ESCA patients with lower ATOH8 levels exhibited significantly shorter overall survival times compared to those with normal tissue levels ($P=0.01$) (Fig. S6B). Additionally, our analysis revealed a negative correlation between FXR1 and ATOH8 mRNA expression levels (Fig. S6C). This interaction was further validated through STRING protein interaction network analysis and GeneMANIA, both of which demonstrated strong connectivity between ATOH8 and the FXR1

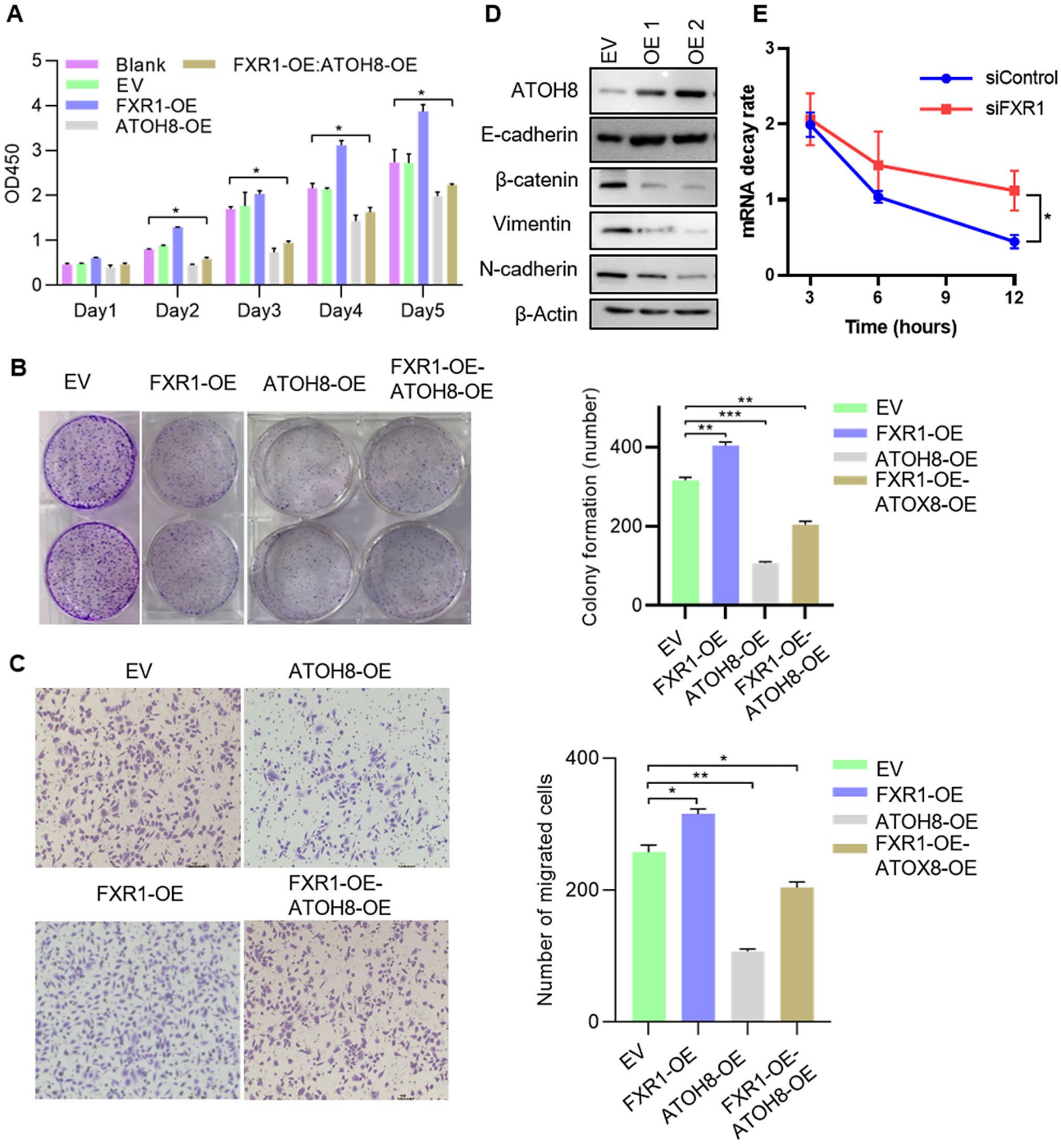

Fig. 7 ATOH8 overexpression inhibited the proliferation and migration of ESCA cell lines. (**A**) ESCA cells were transfected using the ATOH8 overexpression, and cell viability was determined using the CCK-8 assay at indicated time points. Each experiment was performed for 5 days and in triplicates. (**B**) ESCA cells were transfected using the ATOH8 overexpression and subjected to a 6–8 days colony formation assay. The number of colonies was calculated. Scale bar, 100 mm. (**C**) ESCA cells were transfected with ATOH8 overexpression followed by Transwell assay for cell migration. The cells were then observed microscopically (magnification, x200). The relative images and accompanying statistical plots were presented. The experiments were performed in triplicate. (**D**) The expression levels of EMT-related proteins were detected in ATOH8 overexpressed cells by Western blot. β-actin is used as a loading control. (**E**) qRT-PCR analysis revealed the half-life of *ATOH8* mRNA in control or FXR1 knockdown cells after treatment with Actinomycin D. Data is presented as the mean ± SEM ($n = 3$ in each group). *$P < 0.05$, **$P < 0.01$

protein (Fig. S5A, B). Collectively, these findings underscore the role of ATOH8 in counteracting FXR1's effects on ESCA cell progression.

FXR1 is necessary for nuclear stabilization of PDZK1IP1 and ATOH8 mRNAs

To investigate the potential role of FXR1 in the instability of endogenous *PDZK1IP1* and *ATOH8* mRNAs, we treated siControl- or siFXR1-stable transfected OE33 cells with the transcription inhibitor Actinomycin D (ActD) and examined the rate of degradation of *PDZK1IP1* and *ATOH8* mRNAs using qRT-PCR. Intriguingly, the *PDZK1IP1* and *ATOH8* mRNA levels in siControl cells seem to cycle rapidly. In contrast, when FXR1 is depleted, the decay rate of *PDZK1IP1* and *ATOH8* mRNAs is significantly altered, and its half-life is substantially delayed. Consequently, even after 12 h of ActD administration, *PDZK1IP1* and *ATOH8* mRNAs are still expressed. According to our findings, FXR1 deletion enhances the stability of endogenous *PDZK1IP1* and *ATOH8* mRNAs (Figs. 6E and 7E).

FXR1 knockdown and PDZK1IP1 or ATOH8 overexpression suppressed tumor growth

Tumor xenograft models in nude mice have been efficiently developed using OE33 and EC9706 cells. The impact of FXR1 inhibition or PDZK1IP1 and ATOH8 overexpression on the development of esophageal xenograft tumors was then studied. In comparison to the control group, the sh-FXR1, OE-PDZK1IP1+OE-FXR1, and OE-ATOH8+OE-FXR1 groups resulted in considerably lower tumor volumes and weights (Fig. 8A). Furthermore, the sh-FXR1 group had smaller tumor volume and weight than the OE-PDZK1IP1+OE-FXR1 and OE-ATOH8+OE-FXR1 groups, but the tumor inhibitory rate was greater (Fig. 8B-D). In the FXR1 knockdown group, the tumor weight and volume of mice decreased by 80% compared to the scrambled control group ($p<0.01$). Human esophagus xenograft tumors have been stained for CD31, Ki67, and cleaved caspase-3, and these findings are consistent with the in-vivo effects of FXR1 inhibition or PDZK11IP1 and ATOH8 overexpression. The PI value was reduced in the OE-PDZK1IP1 + OE-FXR1 and OE-ATOH8+OE-FXR1 groups compared to the non-treated control group, whereas the AI was higher. In addition, when comparing the sh-FXR1 group to the OE-PDZK1IP1+OE-FXR1 and OE-ATOH8+OE-FXR1 groups, we find that PI is lower in the sh-FXR1 group while the AI is higher (Fig. 8E).

Discussion

RBPs form ribonucleoprotein (RNP) complexes by binding to specific RNAs. Consequently, controlling gene expression processes such as RNA splicing, cleavage and polyadenylation, transport, translation, stability, and degradation of coding RNAs, circular RNAs (circRNA), long non-coding RNAs (lncRNA), and microRNAs (miRNAs), and their precursors [37–39]. This altered activity of FXR1 seems to be present in all cancer types and corresponds with the dysregulation of the related mRNA targets. FXR1, a potential cancer driver gene, is overexpressed in various malignancies. The bioinformatics results of the present study indicate that *FXR1* is an oncogene whose high expression is associated with a low overall survival and recurrence-free survival rate, as well as a poor prognosis in ESCA patients. This observation is consistent with FXR1's involvement in other cancers reported previously [40, 41]. In addition, we discovered that both high-grade ESCA and advanced tumors had considerably elevated FXR1 protein levels.

FXR1's oncogenic functions in numerous human cancers have been progressively recognized and established. This study explored the possibility of FXR1 being linked to ESCA. We initially identified abnormal FXR1 overexpression in our ESCA cell population compared to the normal cell counterpart at both the mRNA and protein levels, indicating a putative oncogenic function for FXR1 in this deadly disease. The suppression of FXR1 through sh-RNA significantly inhibited the proliferation and cell viability and promoted the apoptosis and cellular senescence of OE33 cells. Furthermore, malignant behaviors were attenuated considerably in FXR1-deficient cells, indicating that FXR1 performs multiple functions in the cancer biology of esophageal tumors. Mechanistically, we characterized the increased expression of PDZK1IP1 and ATOH8 at the transcript and protein levels in FXR1-deficient cells. We further unveiled that *PDZK1IP1* and *ATOH8* mRNA stability were improved in OE33 cells after FXR1 knockdown. Our findings, obtained through computational mapping, showed that FXR1 binds to the 3′UTR of *PDZK1IP1* or *ATOH8* and increases its activity in the context of FXR1 deficiency. These results emphasize the potential regulatory action of FXR1 through association with the 3′UTR of *PDZK1IP1* or *ATOH8* transcripts. The direct binding of FXR1 to *PDZK1IP1* or *ATOH8* transcripts was experimentally and reciprocally validated using an RNA-IP assay. We also investigated the specific and pre-dominate roles of PDZK1IP1 and ATOH8 in mediating the oncogenic function of FXR1 in ESCA, and our findings showed that overexpression of PDZK1IP1 or ATOH8 in FXR1-overexpressed cells substantially attenuated the tumor-promoting effects of FXR1 overexpression.

Interestingly, FXR1 inhibition and PDZK1IP1 or ATOH8 overexpression in conjunction with FXR1-overexpressed cells significantly inhibited xenograft tumor development and increased the survival of nude mice. Our findings thus imply that aberrantly high FXR1

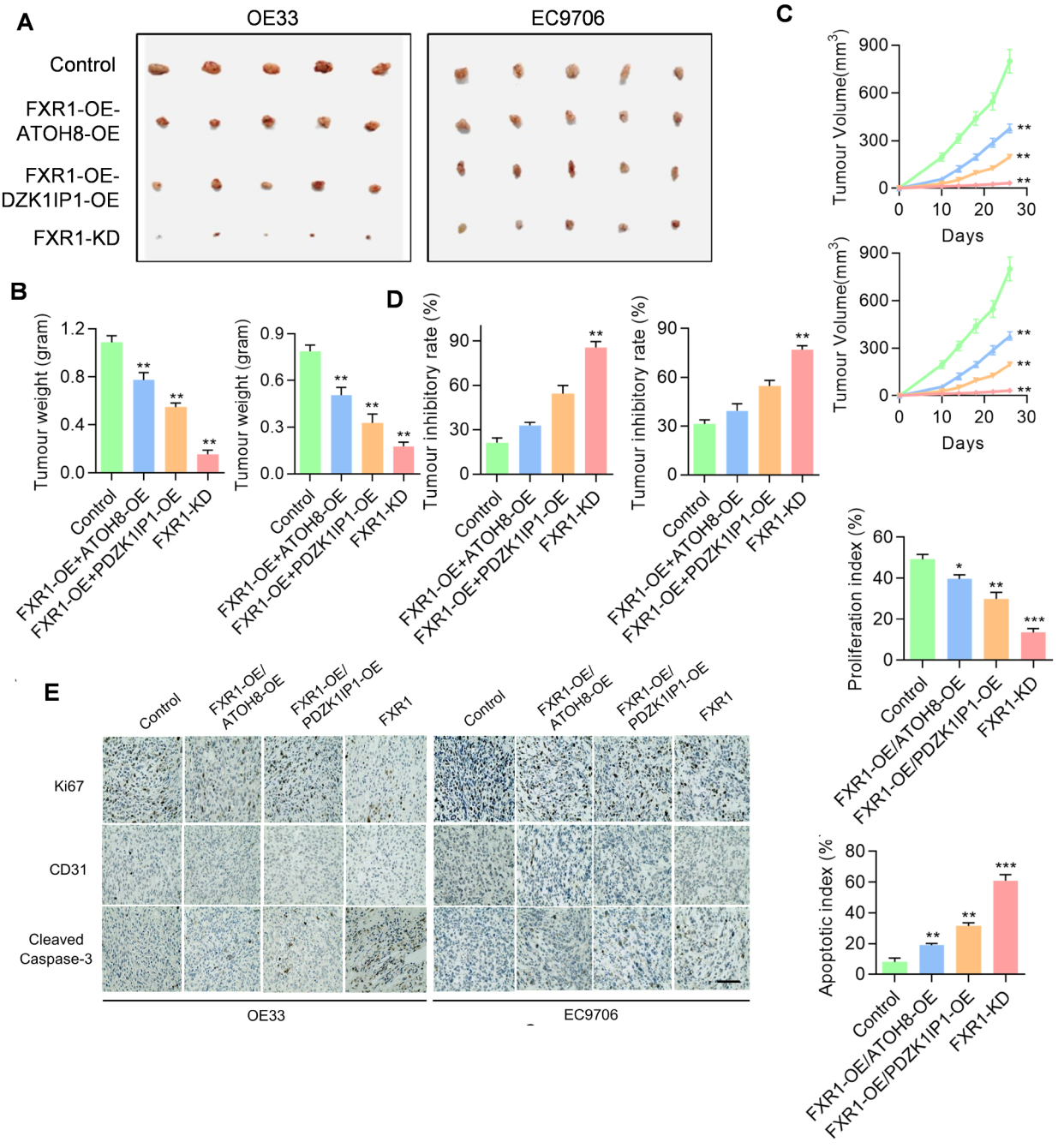

Fig. 8 Effects of FXR1 knockdown, or PDZK1IP1 and ATOH8 overexpression on the growth of human ESCA xenograft tumors in nude mice. (**A**) The representative tumor samples from each group are shown. (**B**) The tumor weight of human ESCA xenograft tumors was measured ($n = 5$). (**C**) The tumor volumes of human ESCA xenograft tumors were measured ($n = 5$). (**D**) The inhibition rate of tumor growth was calculated ($n = 5$). (**E**) Representative photographs of CD31, Ki67, and cleaved caspase-3 staining in human ESCA xenograft tumors (original magnification ×400). The PI, MVD, and AI were calculated ($n = 3$). Data are presented as mean ± SEM. * $p < 0.05$, ** $p < 0.01$ compared with the control group

expression levels, likely via negatively regulating *PDZK1IP1* or *ATOH8* mRNA levels, contribute to the malignant phenotypes in ESCA. For the first time, our findings demonstrate the significance of FXR1-*PDZK1IP1* or FXR1-*ATOH8* signaling in this disease, which may hold significant potential for diagnostic or therapeutic applications.

In the current investigation, we discovered that FXR1 was highly expressed and acts as an oncogene in ESCA cells. FXR1 inhibition reduced the malignant biological characteristics of ESCA cells. Our results are consistent

with its tumor-promoting function in other malignancies. Similar to the findings of this research, FXR1 is ubiquitously expressed and has been linked to a poor prognosis in ovarian and BC [40]. FXR1 is overexpressed in non-small cell lung cancer tissues and cells, knocking down destabilized *ECT2* mRNA, leading to decreased cell proliferation and an increased cell death ratio [41]. Furthermore, in HNSCC, FBXO4-mediated FXR1 degradation reduces carcinogenesis, while FXR1 controls FBXO4 expression in the feedback loop via inhibiting protein translation [32].

Post-transcriptional regulation mechanisms significantly impact eukaryotic gene expression programs, which are often regulated by RBPs via interactions with their 3′UTR region [29]. As crucial regulators of RNA metabolism, RBPs have the potential to have a biological effect by modulating the stability of target RNAs [42–44]. FXR1 plays a crucial role in regulating mRNA stability, and translation by binding to specific RNA sequences and trans-acting elements. It associates with AREs in the 3′-UTR of mRNAs, which are key post-transcriptional regulatory signals, to modify gene expression. FXR1 stabilizes mRNAs by interacting with the miRNA complex or AREs through its KH domains. FXR1 also competes with the RNA-stabilizing protein HuR on ARE-containing transcripts, affecting mRNA decay. Furthermore, FXR1 influences mRNA translation efficiency by interacting with the RNAi pathway and RISC protein AGO2, promoting translation of target mRNAs like *cMYC* [45, 46]. For instance, in OSCC, Majumder et al. showed that FXR1 controlled *p21* and *TERC* RNA to avoid p53-mediated cellular senescence [28]. As was previously mentioned, CPEB4 is abundantly expressed in glioma tissues. Upregulation of CPEB4 increases glioma cell migration and invasion [47]. In BC, increased HuR expression promotes tumorigenesis by enhancing the stability of *ERBB2* mRNA [48]. Meanwhile, osteosarcoma cells had elevated levels of the RNA binding protein Lin28A; knocking it down led to decreased cell proliferation, migration, and invasion, as well as increased cell death by stabilizing the lncRNA *MALAT1* [49]. Fan et al. (2017) demonstrated that FXR1 controlled transcription and was crucial for the development of human cancer with *TP53*/*FXR2* homozygous deletion [50]. In this study, for the first time, we provide clear evidence that *PDZK1IP1* and *ATOH8* are the direct targets of FXR1 for rapid degradation in ESCA cells. FXR1 overexpression destabilizes *PDZK1IP1* and *ATOH8* mRNAs, promoting ESCA development. Mechanistically, FXR1 directly interacts with the 3′-UTRs of these transcripts to promote their degradation. Our findings suggest that FXR1 exerts oncogenic effects through the PDZK1IP1/ATOH8 pathway, indicating potential diagnostic and therapeutic implications. Further studies are needed to validate these results.

PDZK1IP1 is almost exclusively found in kidney epithelial cells in healthy human tissues. However, the dysregulation of PDZK1IP1 has been seen in several human malignancies [14, 15]. Downregulation of PDZK1IP1 has been documented in various tumor types, including ESCA, laryngeal cancer, pancreatic cancer, OSCC, glioma, and prostate cancer [19, 20, 51–53]. Notably, Low levels of PDZK1IP1 expression were linked to tumor growth and were seen in advanced or metastatic tumors. The results of a recent study found that PDZK1IP1 expression was high in normal samples but low in ESCA samples. In a later investigation, age > 60, TNM stage III, and low PDZK1IP1 expression were associated with poor overall survival and unfavorable prognosis [53]. Consistent with these findings, we also observed a low level of PDZK1IP1 expression in ESCA cell lines, which is comparable with the results of previous studies. In addition, overexpression of PDZK1IP1 in the present research suppressed the malignant activity of ESCA cells. In particular, PDZK1IP1 overexpression significantly inhibited ESCA cell migration. We demonstrated that low PDZK1IP1 expression is linked to a worse prognosis, suggesting it may be a potential biomarker for ESCA patients.

The cause of PDZK1IP1 dysregulation in malignant tumors is mostly unknown. We provide evidence that FXR1 overexpression induces PDZK1IP1 dysregulation in ESCA cells. PDZK1IP1 has multifaceted oncogenic actions in various human malignancies, including cell migration [54], tumor development [20], and EMT [55]. In this work, we discovered that overexpression of PDZK1IP1 inhibited the FXR1-induced increase in ESCA cell proliferation and migration. In addition, PDZK1IP1 suppression increased SLUG and vimentin in OSCC cell lines, whereas overexpression decreased N-cadherin, SLUG, and vimentin [20]. Our study found that FXR1 knockdown and PDZK1IP1 overexpression cells had higher E-cadherin expression and lower SLUG, N-cadherin, vimentin, Snail-2, Zeb-1, and SMAD2/3 expression. Thus, it is plausible that FXR1 regulates the expression of EMT-related proteins through the PDZK1IP1 pathway. According to these results, overexpressing PDZK1IP1 in human ESCA cells may be a future strategy for reducing cancer metastasis.

ATOH8 is a new actor in cancer research with ambiguous functions; it was first characterized as an oncogene and later as a tumor suppressor gene in cancers. An examination of the TCGA dataset found that a low level of ATOH8 expression reduces overall survival. In liver cancer cell lines, the overexpression of ATOH8 suppressed proliferation, invasiveness, and migration. Finally, inhibited tumor development while increasing chemoresistance in these cells [56, 57]. In nasopharyngeal carcinomas, inhibition of ATOH8 promoted the malignant phenotype, whereas transgenic expression restored its function [58]. Similarly, ATOH8 is downregulated in bladder, lung,

prostate, and ovarian cancers [59]. Consistent with other studies, our results showed that ATOH8 overexpression suppressed the malignant activity of ESCA cells. Specifically, overexpression of ATOH8 significantly inhibited the growth and migration of ESCA cells. Additionally, it was shown that overexpression of ATOH8 suppressed the FXR1-induced proliferation and migration of ESCA cells. In addition, we observed an association between EMT markers and ATOH8, indicating that this novel emergent transcription factor is likely a bona fide EMT regulator whose expression is remarkably reduced by exogenous FXR1 to facilitate ESCA growth. When ATOH8 was overexpressed, we observed an upregulation of the epithelial marker E-cadherin and a downregulation of the mesenchymal markers β-catenin, vimentin, and N-cadherin.

Further investigation is warranted to comprehensively understand the therapeutic potential of targeting FXR1-PDZK1IP1/ATOH8 signaling in ESCA murine models. Additionally, it is important to explore the impact of FXR1 knockdown on the expression levels of PDZK1IP1 and ATOH8 in other cancers to validate their roles in ESCA progression. FXR1 may also directly regulate numerous other mRNAs, which could be elucidated using unbiased genome-wide analyses such as eCLIP-seq. Identifying all potential targets of FXR1 and testing the efficacy of FXR1 inhibition for cancer therapy are crucial steps for future research.

In conclusion, we studied the expression of FXR1, PDZK1IP1, and ATOH8 in ESCA cells and discovered the underlying molecular pathways. We provide the first comprehensive overview of FXR1 abnormal expression contributing to ESCA. The depletion of FXR1 is significantly associated with anti-tumor characteristics, such as the inhibition of cell proliferation and viability, suppression of migration, and the promotion of apoptosis and cellular senescence. We were further mechanistically explicit that FXR1 regulates PDZK1IP1 and ATOH8 expression via interacting with its 3′UTR, and the dominant distinct function of both PDZK1IP1 and ATOH8 in this signaling pathway is underlined. Our findings show that FXR1 has oncogenic activities through the PDZK1IP1/ATOH8 pathway. These findings imply that FXR1-*PDZK1IP1* or FXR1-*ATOH8* have significant potential as diagnostic or therapeutic improvements.

Abbreviations

AI	Apoptosis index
AP	Ammonium persulfate
AREs	AU-rich elements
ASO	Anti-sense oligo
ATOH8	Atonal homolog 8
BHLH	Basic helix-loop-helix
CCK-8	Cell counting Kit-8
CDS	Coding sequence
CD31	Cluster of differentiation 31
cMYC	MYC proto-oncogene
CNV	Copy number variants
ECL	Enhanced chemiluminescence
EMT	Epithelial-mesenchymal transition
ESCA	Esophagus cancer
FBS	Fetal bovine serum
FBXO4	F-Box Protein 4
FXR1	Fragile X-related protein 1
HE	Hematoxylin and eosin
IHC	Immunohistochemistry
IR	Inhibition rate
KD	Knockdown
miRNAs	Micro RNAs
OD	Optical density
OE	Overexpression
ORF	Open reading frame
PBS	Phosphate buffered saline
PDZK1IP1	PDZK1-interacting protein 1
PI	Proliferation index
MVD	Microvessel density
qRT-PCR	Quantitative real time PCR
RBPs	RNA binding protein
RNP	Ribonucleoprotein
RNA-IP	RNA-immunoprecipitation
SEM	Standard error of the mean
SNP	Single nucleotide polymorphism
TGF-β	Transforming growth factor beta
UTR	Untranslated region

Supplementary Information

The online version contains supplementary material available at https://doi.org/10.1186/s13062-024-00553-3.

Supplementary Mtaerial 1

Supplementary Fig. S1: Bioinformatic analysis of FXR1 expression in cancers. (A) The left panel of a box-plot displays the relationship between the copy number changes in the FXR1 mRNA and the protein in the right panel. The two-sided Wilcoxon rank-sum test was used to get the p-value. (B) The most prevalent mutation of FXR1 in cancers is amplification. (C) FXR1 protein expression is positively associated with stage (left) and grade (right) of esophageal tumor growth. The error bars show the median +SD. Significance was determined by two-sided Wilcoxon rank sum test where $^{**}p<0.01$, $^{***}p<0.001$

Supplementary Fig. S2: Effects of FXR1 overexpression on proliferation of human ESCA cells. The DNA replication activities were examined by EdU assay (original magnification × 200). The experiments were performed in triplicate. Data are presented as mean ± SEM. * $p < 0.05$, ** $p < 0.01$ compared with the control group

Supplementary Fig. S3: Effects of FXR1 overexpression on migration of human ESCA cells. Cell migration was measured by scratch assay (original magnification × 100). The number of migrated cells was calculated. The experiments were performed in triplicate. Data are presented as mean ± SEM. * $p < 0.05$, ** $p < 0.01$ compared with the control group

Supplementary Fig. S4: Bioinformatic analysis of PDZK1IP1 expression in cancers. (A) Violin plot for PDZK1IP1 expression level between tumors vs. normal cases in ESCA. (B) Multivariate Cox analysis of the PDZK1IP1 gene. (C) FXR1 and PDZK1IP1 correlation scatter plot. Log2 [TPM] represents gene expression levels. Data are presented as mean ± SEM. * $p < 0.05$, ** $p < 0.01$ compared with the control group

Supplementary Fig. S5: FXR1 Interaction with PDZK1IP1 and ATOH8 gene. (A) Protein-protein interactions were created in STRING for the two genes selected for further studies. (B) Interaction of FXR1, PDZK1IP1 and ATOH8 was created by GeneMANIA (a database for the identification of co-expression genes)

Supplementary Fig. S6: Bioinformatic analysis of ATOH8 expression in cancers. (A, B) ATOH8 expression profile and overall survival of ESCA in the TCGA datasets. (C) FXR1 and ATOH8 correlation scatter plot. Log2 [TPM] represents gene expression levels. Data are presented as mean ± SEM. * $p < 0.05$, ** $p < 0.01$ compared with the control group

Acknowledgements
Not applicable.

Author contributions
FAK conducted research and drafted the original manuscript. FAK, DF, FSA and SJ assisted in the process of designing the experiments, revising the manuscript and the construction of the figures and tables. SJ contributed to the conceptual framework. JD, SJ, and NF supervised the study and revised the manuscript. All authors listed have made a substantial, direct, and intellectual contribution to the work and have been approved for publication.

Funding
This work was supported by the National Natural Science Foundation of China (No.31371386) and the Researchers Supporting Project number (RSPD2024R693), King Saud University, Riyadh, Saudi Arabia.

Data availability
No datasets were generated or analysed during the current study.

Declarations

Ethics approval and consent to participate
Not applicable.

Consent for publication
All authors consent to publication.

Informed consent
The Committee of Medical Ethics and Welfare for Experimental Animals of Henan University School of Medicine (HUSOM-2022–165) approved the animal experiment in compliance with the guidelines of the Basel Declaration.

Institutional review board statement
Not applicable.

Competing interests
The authors declare no competing interests.

Received: 12 September 2024 / Accepted: 28 October 2024
Published online: 07 November 2024

References

1. Re A, Joshi T, Kulberkyte E, Morris Q, Workman CT. RNA-protein interactions: an overview. Methods Mol Biol. 2014;1097:491–521. https://doi.org/10.1007/978-1-62703-709-9_23.
2. Gerstberger S, Hafner M, Tuschl T. A census of human RNA-binding proteins. Nat Rev Genet. 2014;15(12):829–45. https://doi.org/10.1038/nrg3813.
3. Pereira B, Billaud M, Almeida R. RNA-Binding proteins in Cancer: old players and New actors. Trends Cancer. 2017;3(7):506–28. https://doi.org/10.1016/j.trecan.2017.05.003.
4. Hentze MW, Castello A, Schwarzl T, Preiss T. A brave new world of RNA-binding proteins. Nat Rev Mol Cell Biol. 2018;19(5):327–41. https://doi.org/10.1038/nrm.2017.130.
5. George J, Li Y, Kadamberi IP, Parashar D, Tsaih SW, Gupta P et al. RNA-binding protein FXR1 drives cMYC translation by recruiting eIF4F complex to the translation start site. Cell Rep. 2021; 37(5):109934. https://doi.org/10.1016/j.celrep.2021.109934. Erratum in: Cell Rep. 2023; 42(3):112228.
6. Bechara E, Davidovic L, Melko M, Bensaid M, Tremblay S, Grosgeorge J, et al. Fragile X related protein 1 isoforms differentially modulate the affinity of fragile X mental retardation protein for G-quartet RNA structure. Nucleic Acids Res. 2007;35(1):299–306. https://doi.org/10.1093/nar/gkl1021.
7. Schaeffer C, Bardoni B, Mandel JL, Ehresmann B, Ehresmann C, Moine H. The fragile X mental retardation protein binds specifically to its mRNA via a purine quartet motif. EMBO J. 2001;20(17):4803–13. https://doi.org/10.1093/emboj/20.17.4803.
8. Vasudevan S, Steitz JA. AU-rich-element-mediated upregulation of translation by FXR1 and Argonaute 2. Cell. 2007;128(6):1105–18. https://doi.org/10.1016/j.cell.2007.01.038.
9. Darnell JC, Fraser CE, Mostovetsky O, Darnell RB. Discrimination of common and unique RNA-binding activities among fragile X mental retardation protein paralogs. Hum Mol Genet. 2009;18(17):3164–77. https://doi.org/10.1093/hmg/ddp255.
10. Tamanini F, Willemsen R, van Unen L, Bontekoe C, Galjaard H, Oostra BA, et al. Differential expression of FMR1, FXR1 and FXR2 proteins in human brain and testis. Hum Mol Genet. 1997;6(8):1315–22. https://doi.org/10.1093/hmg/6.8.1315.
11. Zarnescu DC, Gregorio CC. Fragile hearts: new insights intotranslational control in cardiac muscle. Trends Cardiovasc Med. 2013;23(8):275–81. https://doi.org/10.1016/j.tcm.2013.03.003.
12. Kocher O, Cheresh P, Lee SW. Identification and partial characterization of a novel membrane-associated protein (MAP17) up-regulated in human carcinomas and modulating cell replication and tumor growth. Am J Pathol. 1996;149(2):493–500.
13. Jaeger C, Schaefer BM, Wallich R, Kramer MD. The membrane-associated protein pKe#192/MAP17 in human keratinocytes. J Invest Dermatol. 2000;115(3):375–80. https://doi.org/10.1046/j.1523-1747.2000.00071.x.
14. Guijarro MV, Castro ME, Romero L, Moneo V, Carnero A. Large scale genetic screen identifies MAP17 as protein bypassing TNF-induced growth arrest. J Cell Biochem. 2007;101(1):112–21. https://doi.org/10.1002/jcb.21163.
15. Guijarro MV, Leal JF, Fominaya J, Blanco-Aparicio C, Alonso S, Lleonart M, et al. MAP17 overexpression is a common characteristic of carcinomas. Carcinogenesis. 2007;28(8):1646–52. https://doi.org/10.1093/carcin/bgm083.
16. Guijarro MV, Link W, Rosado A, Leal JF, Carnero A. MAP17 inhibits myc-induced apoptosis through PI3K/AKT pathway activation. Carcinogenesis. 2007;28(12):2443–50. https://doi.org/10.1093/carcin/bgm154.
17. de Miguel-Luken MJ, Chaves-Conde M, de Miguel-Luken V, Muñoz-Galván S, López-Guerra JL, et al. MAP17 (PDZKIP1) as a novel prognostic biomarker for laryngeal cancer. Oncotarget. 2015;6(14):12625–36. https://doi.org/10.18632/oncotarget.3470.
18. Ferrer I, Quintanal-Villalonga Á, Molina-Pinelo S, Garcia-Heredia JM, Perez M, Suárez R, et al. MAP17 predicts sensitivity to platinum-based therapy, EGFR inhibitors and the proteasome inhibitor bortezomib in lung adenocarcinoma. J Exp Clin Cancer Res. 2018;37(1):195. https://doi.org/10.1186/s13046-018-0871-7.
19. Ikeno S, Nakano N, Sano K, Minowa T, Sato W, Akatsu R, et al. PDZK1-interacting protein 1 (PDZK1IP1) traps Smad4 protein and suppresses transforming growth factor-β (TGF-β) signaling. J Biol Chem. 2019;294(13):4966–80. https://doi.org/10.1074/jbc.RA118.004153.
20. Guijarro MV, Leal JF, Blanco-Aparicio C, Alonso S, Fominaya J, Lleonart M (d), et al. editors. MAP17 enhances the malignant behavior of tumor cells through ROS increase. Carcinogenesis. 2007; 28(10):2096 – 104. https://doi.org/10.1093/carcin/bgm124
21. Chen J, Dai F, Balakrishnan-Renuka A, Leese F, Schempp W, Schaller F, et al. Diversification and molecular evolution of ATOH8, a gene encoding a bHLH transcription factor. PLoS ONE. 2011;6(8):e23005. https://doi.org/10.1371/journal.pone.0023005.
22. Fang F, Wasserman SM, Torres-Vazquez J, Weinstein B, Cao F, Li Z, et al. The role of Hath6, a newly identified shear-stress-responsive transcription factor, in endothelial cell differentiation and function. J Cell Sci. 2014;127(Pt 7):1428–40. https://doi.org/10.1242/jcs.136358.
23. Bersten DC, Sullivan AE, Peet DJ, Whitelaw ML. bHLH-PAS proteins in cancer. Nat Rev Cancer. 2013;13(12):827–41. https://doi.org/10.1038/nrc3621.
24. Ducray F, Idbaih A, de Reyniès A, Bièche I, Thillet J, Mokhtari K, et al. Anaplastic oligodendrogliomas with 1p19q codeletion have a proneural gene expression profile. Mol Cancer. 2008;7:41. https://doi.org/10.1186/1476-4598-7-41.
25. Song Y, Pan G, Chen L, Ma S, Zeng T, Man Chan TH, et al. Loss of ATOH8 increases stem cell features of Hepatocellular Carcinoma cells. Gastroenterology. 2015;149(4):1068–e815. https://doi.org/10.1053/j.gastro.2015.06.010.
26. Wang Z, Xie J, Yan M, Wang J, Wang X, Zhang J, et al. Downregulation of ATOH8 induced by EBV-encoded LMP1 contributes to the malignant phenotype of nasopharyngeal carcinoma. Oncotarget. 2016;7(18):26765–79. https://doi.org/10.18632/oncotarget.8503.
27. Zhao F, Yu J. Unearthing a novel tumor suppressor function of ATOH8 in hepatocellular carcinoma: role in acquisition of cancer stem cell-like features. Cancer Res. 2016;5:S91–4. https://doi.org/10.21037/tcr.2016.05.02.
28. Majumder M, House R, Palanisamy N, Qie S, Day TA, Neskey D, et al. RNA-Binding protein FXR1 regulates p21 and TERC RNA to Bypass p53-Mediated Cellular Senescence in OSCC. PLoS Genet. 2016;12(9):e1006306. https://doi.org/10.1371/journal.pgen.1006306.

29. Comeau SR, Gatchell DW, Vajda S, Camacho CJ. ClusPro: an automated docking and discrimination method for the prediction of protein complexes. Bioinformatics. 2004;20(1):45–50. https://doi.org/10.1093/bioinformatics/btg371.
30. Jin X, Zhai B, Fang T, Guo X, Xu L. FXR1 is elevated in colorectal cancer and acts as an oncogene. Tumour Biol. 2016;37(2):2683–90. https://doi.org/10.1007/s13277-015-4068-9.
31. Comtesse N, Keller A, Diesinger I, Bauer C, Kayser K, Huwer H, et al. Frequent overexpression of the genes FXR1, CLAPM1 and EIF4G located on amplicon 3q26-27 in squamous cell carcinoma of the lung. Int J Cancer. 2007;120(12):2538–44. https://doi.org/10.1002/ijc.22585.
32. Qie S, Majumder M, Mackiewicz K, Howley BV, Peterson YK, Howe PH, et al. Fbxo4-mediated degradation of Fxr1 suppresses tumorigenesis in head and neck squamous cell carcinoma. Nat Commun. 2017;8(1):1534. https://doi.org/10.1038/s41467-017-01199-8.
33. Gao P, Liu H, Yang Z, Hui Y, Shi Z, Yang Z, et al. Development of a Novel highly spontaneous metastatic model of esophageal squamous cell carcinoma using renal Capsule Technology. Onco Targets Ther. 2021;14:785–93. https://doi.org/10.2147/OTT.S290564.
34. Mbagwu SI, Filgueira L. Differential expression of CD31 and Von Willebrand Factor on Endothelial Cells in different regions of the human brain: potential implications for cerebral malaria pathogenesis. Brain Sci. 2020;10(1):31. https://doi.org/10.3390/brainsci10010031.
35. Lanng MB, Møller CB, Andersen AH, Pálsdóttir ÁA, Røge R, Østergaard LR, et al. Quality assessment of Ki67 staining using cell line proliferation index and stain intensity features. Cytometry A. 2019;95(4):381–8. https://doi.org/10.1002/cyto.a.23683.
36. Kobayashi T, Masumoto J, Tada T, Nomiyama T, Hongo K, Nakayama J. Prognostic significance of the immunohistochemical staining of cleaved caspase-3, an activated form of caspase-3, in gliomas. Clin Cancer Res. 2007;13(13):3868–74. https://doi.org/10.1158/1078-0432.CCR-06-2730.
37. Khan FA, Nsengimana B, Khan NH, Song Z, Ngowi EE, Wang Y, et al. Chimeric Peptides/Proteins encoded by circRNA: an update on mechanisms and functions in human cancers. Front Oncol. 2022;12:781270. https://doi.org/10.3389/fonc.2022.781270.
38. Khan FA, Nsengimana B, Khan NH, Huang J, Guo H, Awan UA, et al. Differential expression profiles of circRNAs in cancers: future clinical and diagnostic perspectives. Gene Protein Dis. 2022;1(2):138. https://doi.org/10.36922/gpd.v1i2.138.
39. Khan FA, Fang N, Zhang W, Ji S. The multifaceted role of Fragile X-Related protein 1 (FXR1P) in Cellular processes: an updated review on Cancer and clinical applications. Cell Death Dis. 2024;15:72. https://doi.org/10.1038/s41419-023-06413-8.
40. Chai C, Wu H, Wang B, Eisenstat DD, Leng RP. MicroRNA-498 promotes proliferation and migration by targeting the tumor suppressor PTEN in breast cancer cells. Carcinogenesis. 2018;39(9):1185–96. https://doi.org/10.1093/carcin/bgy092.
41. Qian J, Hassanein M, Hoeksema MD, Harris BK, Zou Y, Chen H, et al. The RNA binding protein FXR1 is a new driver in the 3q26-29 amplicon and predicts poor prognosis in human cancers. Proc Natl Acad Sci U S A. 2015;112(11):3469–74. https://doi.org/10.1073/pnas.1421975112.
42. Khan FA, Nsengimana B, Awan UA, Ji XY, Ji S, Dong J. Regulatory roles of N6-methyladenosine (m6A) methylation in RNA processing and non-communicable diseases. Cancer Gene Ther. 2024. https://doi.org/10.1038/s41417-024-00789-1.
43. Ankö ML, Neugebauer KM. RNA-protein interactions in vivo: global gets specific. Trends Biochem Sci. 2012;37(7):255–62. https://doi.org/10.1016/j.tibs.2012.02.005.
44. Hong S. RNA binding protein as an emerging therapeutic target for Cancer Prevention and Treatment. J Cancer Prev. 2017;22(4):203–10. https://doi.org/10.15430/JCP.2017.22.4.203.
45. Espel E. The role of the AU-rich elements of mRNAs in controlling translation. Semin Cell Dev Biol. 2005;16:59–67. https://doi.org/10.1016/j.semcdb.2004.11.008. (Academic Press).
46. Nsengimana B, Khan FA, Ngowi EE, Zhou X, Jin Y, Jia Y, et al. Processing body (Pbody) and its mediators in cancer. Mol Cell Biochem. 2022. https://doi.org/10.1007/s11010-022-04359-7.
47. Zhijun L, Dapeng W, Hong J, Guicong W, Bingjian Y, Honglin L. Overexpression of CPEB4 in glioma indicates a poor prognosis by promoting cell migration and invasion. Tumour Biol. 2017;39(4):1010428317694538. https://doi.org/10.1177/1010428317694538.
48. Tan S, Ding K, Chong QY, Zhao J, Liu Y, Shao Y, et al. Post-transcriptional regulation of ERBB2 by miR26a/b and HuR confers resistance to tamoxifen in estrogen receptor-positive breast cancer cells. J Biol Chem. 2017;292(33):13551–64. https://doi.org/10.1074/jbc.M117.780973.
49. Wang Z, Pang J, Ji B, Zhang S, Cheng Y, Yu L, et al. RNA binding protein Lin28A promotes osteocarcinoma cells progression by associating with the long noncoding RNA MALAT1. Biotechnol Lett. 2018;40(3):493–500. https://doi.org/10.1007/s10529-017-2489-9.
50. Fan Y, Yue J, Xiao M, Han-Zhang H, Wang YV, Ma C, et al. FXR1 regulates transcription and is required for growth of human cancer cells with TP53/FXR2 homozygous deletion. Elife. 2017;6:e26129. https://doi.org/10.7554/eLife.26129.
51. Uhlén M, Fagerberg L, Hallström BM, Lindskog C, Oksvold P, Mardinoglu A, et al. Proteomics. Tissue-based map of the human proteome. Science. 2015;347(6220):1260419. https://doi.org/10.1126/science.1260419.
52. Hsiao SY, Weng SM, Hsiao JR, Wu YY, Wu JE, Tung CH, et al. MiR-455-5p suppresses PDZK1IP1 to promote the motility of oral squamous cell carcinoma and accelerate clinical cancer invasion by regulating partial epithelial-to-mesenchymal transition. J Exp Clin Cancer Res. 2023;42(1):40. https://doi.org/10.1186/s13046-023-02597-1.
53. Liu K, Jiao YL, Shen LQ, Chen P, Zhao Y, Li MX, et al. A prognostic model based on mRNA expression analysis of esophageal squamous cell carcinoma. Front Bioeng Biotechnol. 2022;10:823619. https://doi.org/10.3389/fbioe.2022.823619.
54. Chen X, Liao Y, Yu Y, Zhu P, Li J, Qin L, et al. Elevation of MAP17 enhances the malignant behavior of cells via the Akt/mTOR pathway in hepatocellular carcinoma. Oncotarget. 2017;8(54):92589–603. https://doi.org/10.18632/oncotarget.21506.
55. García-Heredia JM, Otero-Albiol D, Pérez M, Pérez-Castejón E, Muñoz-Galván S, Carnero A. Breast tumor cells promotes the horizontal propagation of EMT, stemness, and metastasis by transferring the MAP17 protein between subsets of neoplastic cells. Oncogenesis. 2020;9(10):96. https://doi.org/10.1038/s41389-020-00280-0.
56. Huang Q, Li S, Hu X, Sun M, Wu Q, Dai H, et al. Shear stress activates ATOH8 via autocrine VEGF promoting glycolysis dependent-survival of colorectal cancer cells in the circulation. J Exp Clin Cancer Res. 2020;39(1):25. https://doi.org/10.1186/s13046-020-1533-0.
57. Chen L, Yang J, Wang Y, Wu N, Li X, Li J, et al. ATOH8 overexpression inhibits the tumor progression and monocyte chemotaxis in hepatocellular carcinoma. Int J Clin Exp Pathol. 2020;13(10):2534–43.
58. Ye M, He Y, Lin H, Yang S, Zhou Y, Zhou L, et al. High expression of atonal homolog 8 predicts a poor clinical outcome in patients with colorectal cancer and contributes to tumor progression. Oncol Rep. 2017;37(5):2955–63. https://doi.org/10.3892/or.2017.5554.
59. Cao H, Gao R, Yu C, Chen L, Feng Y. The RNA-binding protein FXR1 modulates prostate cancer progression by regulating FBXO4. Funct Integr Genomics. 2019;19(3):487–96. https://doi.org/10.1007/s10142-019-00661-8.

Publisher's note